ENTROPY-BASED FUZZY CLUSTERING ALGORITHM FOR BRAIN MR IMAGE SEGMENTATION

Project submitted to

FACULTY OF ENGINEERING AND TECHNOLOGY

JADAVPUR UNIVERSITY

In partial fulfillment of the requirements for the degree of

MASTER OF COMPUTER APPLICATIONS, 2018

BY

Riya Patra

Examination Roll: MCA186004

Registration No: 133666 of 2015-2016

Under the guidance of

Dr. Jamuna Kanta Sing

Professor, Department of Computer Science Engineering

Jadavpur University

DEPARTMENT OF COMPUTER SCIENCE AND ENGINEERING

FACULTY OF ENGINEERING AND TECHNOLOGY

JADAVPUR UNIVERSITY

TO WHOM IT MAY CONCERN

I hereby recommend that the project entitled "Entropy-based Fuzzy Clustering Algorithm for Brain MR Image Segmentation" prepared under my supervision and guidance at Jadavpur University, Kolkata by RIYA PATRA *(Reg. No. 133666 of 2015 – 16, Class Roll No. 001510503004), may be accepted in partial fulfillment for the degree of Master of Computer Applications in the Faculty of Engineering and Technology, Jadavpur University, during the academic year 2017 – 2018. I wish him every success in life.*

……..
Prof. (Dr.) Ujjwal Maulik
Head of the Department
Department of Computer Science and Engineering
Jadavpur University, Kolkata – 700032.

……
Prof. (Dr.) Jamuna Kanta Sing
Project Supervisor,
Department of Computer Science and Engineering
Jadavpur University, Kolkata – 700032.

……..
Prof. (Dr.) Chiranjib Bhattacharjee
Dean, Faculty council of Engg. & Tech.
Jadavpur University, Kolkata – 700032.

DECLARATION OF ORIGINALITY AND COMPLIANCE OF ACADEMIC PROJECT

I hereby declare that this project contains literature survey and original research work by the undersigned candidate, as part of her MASTER OF COMPUTER APPLICATIONS studies. All information in this document have been obtained and presented in accordance with academic rules and ethical conduct. I also declare that, as required by these rules and conduct, I have fully cited and referenced all material results that are not original to this work.

NAME: RIYA PATRA

ROLL NUMBER: 001510503004

PROJECT TITLE: Entropy-based Fuzzy Clustering Algorithm for Brain MR Image Segmentation

SIGNATURE WITH DATE:

JADAVPUR UNIVERSITY
FACULTY OF ENGINEERING AND TECHNOLOGY

CERTIFICATE OF APPROVAL

The forgoing project is hereby accepted as a credible study of an engineering subject carried out and presented in a manner satisfactory to warrant its acceptance as a prerequisite to the degree for which it has been submitted. It is understood that by this approval the undersigned do not necessarily endorse or approve any statement made, opinion expressed or conclusion drawn therein, but approve the project only for the purpose for which it is submitted.

FINAL EXAMINATION FOR
EVALUATION OF PROJECT: 1._____

2._____

(Signature of Examiners)

ACKNOWLEDGEMENT

I express my honest and sincere thanks and humble gratitude to my respected teacher and guide *Prof. (Dr.) Jamuna Kanta Sing*, Professor of the Department of Computer Science & Engineering, Jadavpur University, for his exclusive guidance and entire support in completing and producing this project successfully. I am very much indebted to him for the constant encouragement, and continuous inspiration that he has given to me. The above words are only a token of my deep respect towards him for all he has done to take my project to the present shape.

I would like to thank *Ms. Nabanita Mahata* for valuable support and suggestions to the activities of the project.

Finally, I convey my real sense of gratitude and thankfulness to my family members, specially my elder sister, for being an endless source of optimism and positive thoughts; and last but not the least, my father & mother for their unconditional support, without which I would hardly be capable of producing this huge work.

RIYA PATRA
Examination Roll: MCA186004
Registration No: 133666 of 2015 – 2016

TABLE OF CONTAINS

CHAPTER 1
INTRODUCTION

1.1. Image segmentation:

The image segmentation is referred to as one of the most important process of image processing. It is the technique where an image is divided or partitioned into disjoint parts which have similar features and properties, called segments. The main aim of segmentation is simplification which is nothing but representing an image into meaningful and easily analyzable way depending upon its intensity, color and texture [1]. Segmentation has two objectives. The first one is to decompose the image into parts for further analysis. The second one is to perform a change of representation. Image segmentation is the most important task in medical image analysis [2] and is often the first and the most critical step in many clinical applications.

1.2. Brain MR image segmentation:

In brain MR (magnetic resonance) image analysis, image segmentation is commonly used for measuring and visualizing the brain's anatomical structures, for analyzing brain changes, delineating pathological regions, and for surgical planning and image guided intervention. This diversity of image processing application has led to development of various segmentation techniques of different accuracy and degree of complexity [3].

2D-images:

Fig. 1: 2D-MR brain image

An image can be defined as a function *I (i, j)* in 2D space where $i = 0,\ldots\ldots, M\text{-}1$, $j = 1,\ldots\ldots, N\text{-}1$ denote spatial coordinates. The values of the function *I (i, j)* is the intensity values and typically represented by a grey value {0, ……., 255} in MR (magnetic resonance) image of the brain.

Every image consists of a finite set of image elements, called pixels in 2D-space. Each image element is uniquely specified by its intensity value and its coordinates, *(i, j)* for pixels where *i* is the image row number and *j* is the column number [3].

	(i, j)		

In the case of brain MR (magnetic resonance) image elements are typically classified into three main tissue types: cerebrospinal fluid (CSF), grey matter (GM), white matter (WM) [4]. Most of the image segmentation methods are focused on 2D-images.

1.3. Types of segmentation methods:

There are a lot of algorithms for segmentation of medical images such as, MR images used popularly in the past. Intensity thresholding, region-based segmentation, edge-based

segmentation and classification-based segmentation are such techniques which have been used regularly for segmenting MR images [5-7].

The grey level histogram of the image is considered as the threshold level in Intensity thresholding. The disadvantage of intensity thresholding method is to determine the optimal threshold. On the other hand, another disadvantage of intensity thresholding is spatial uncertainty as the pixel location information is ignored [8].

In the edge-based segmentation technique, interrupted or scattered contour lines are created around an object of interest using some edge detection algorithms. Therefore, these contour lines joined based on some similarity criteria to detect the object of region of interest (ROI). However, these methods are computationally expensive for obtaining hole free representation of the objects. The region based segmentation methods extend the thresholding by integrating it with connectivity by means of an intensity similarity measure. The main aim of these above mentioned methods is to get connected regions based on homogeneity criteria of neighbourhood pixels. These are sensitive to noise [9] and less suitable for medical image segmentation.

In classification-based segmentation method, the fuzzy C-means (FCM) clustering algorithm [10], is more effective than other hard clustering methods, like k-means algorithm etc. The FCM algorithm is more reasonable in real applications because it allows pixels to have relation with multiple clusters with varying degree of memberships. FCM is no doubt a very popular unsupervised clustering method, but it has some serious disadvantages due to consideration of the image spatial information. It has another drawback of local optimal solution due to poor initialization. Many modified fuzzy clustering approaches have been reported in the past for making the FCM algorithm more robust to noise and outliers for image segmentation [11-27]. Pedrycz [11] introduced a conditional fuzzy C-means based clustering method guided by an auxiliary or conditional variable. The method reveals a structure within a family of patterns by considering their vicinity in a feature space along with the similarity of the values assumed by a certain conditional variable. Mohamed et al. [13] modified the FCM algorithm through the incorporation of the spatial information. They introduced the spatial information into the computation of similarity measure. The similarity measure is modified to drag a pixel closure to the cluster center if it is in homogeneous region. The drawbacks of this algorithm are its sensitivity to the non-descriptive initial centers and its massively computational loads.

Ahmed et al. [14] introduced the local grey level information by modifying the objective function with another similarity measure for bias field estimation and segmentation of MRI data. This method is also expensive in terms of computational time. Many researchers subsequently modified the objective functions and develop several robust FCM variants for image segmentation [15-22]. These algorithms are shown to have better performances than the standard FCM algorithm. However, some of these methods depend on a fixed spatial factor which needs to be adjusted according to the real applications. In order to overcome the problem of over-smoothed edges, causes due to use of larger spatial window, adaptive selection mechanisms of the spatial parameters have been proposed [23-25]. The performances of these methods are superior and are able to reduce partly the blurring effects which arise due to use of filtering and larger spatial window. Another major contribution with spatial information into the FCM membership function was suggested by Chuang et al. [26], known as sFCM algorithm. The spatial function is the summation of the membership function in the neighborhood of each pixel under consideration. It represents the probability for a pixel to belong into a particular cluster. This spatial function is incorporated into a weighted membership function. The advantages of this method are; it yields regions more homogeneous than those of other methods and it removes the noisy spots and partly reduces the spurious blobs.

Recently, Qiu et al. [27] suggested a novel algorithm for fuzzy segmentation by introducing two fuzzifiers and a spatial constraint in the membership function. Benaichouche et al. [28] presented another improvement of the FCM clustering algorithm using particle swarm optimization (PSO) initialization, Mahalanobis distance and post segmentation correction. The first step introduced PSO initialization to overcome the of the solution in local minima, the second step was concerned with the integration of the spatial grey level information and the Mahalanobis distance and the final step refined the segmentation results by reallocating the potentially misclassified pixels. Kannan et al. [29] introduced a class of robust non-Euclidean distance measure for the objective function to enhance the robustness of the original FCM clustering algorithm and to reduce noise and outliers. Liao et al. [30] proposed a fast spatial constrained fuzzy kernel FCM (FKFCM) algorithm for MR brain image segmentation. The FKFCM algorithm first transforms the pixel intensities into a higher dimensional space using a kernel trick and then performs classification on the transformed data.

Selvathi et al. [31] presented a modified version of spatial FCM algorithm to classify the pixels. Adhikari et al. [32] presented a method for MRI brain image segmentation by incorporating intensity inhomogeneity (IIH) and spatial information by using probabilistic FCM algorithm. The method works in two steps. First, it estimates the intensity inhomogeneity by fusing Gaussian surfaces and subsequently generates the IIH-corrected image. In the second step, it classifies the pixels of the IIH-corrected image by a probabilistic FCM algorithm.

Most of the methods discussed so far suffer heavily due to presence of noise and another additional multiplicative noise factor called intensity inhomogeneity (IIH) or bias field in the MR medical images. The IIH usually refers to the slow, non-anatomic intensity variations of the same tissue over the image domain and causes due to imperfection of the image acquisition devices, eddy current, poor magnetic field and patient movement etc.

1.3. Proposed method:

In our proposed method we incorporate Shannon entropy with conventional FCM algorithm that can effectively segment MR brain images with the presence of noise and intensity inhomogeneity (IIH). Entropy is involved as the dissimilarity among the pixels in the regions along the edges is very high.

CHAPTER 2

PROPOSED ENTROPY-BASED FUZZY CLUSTERING ALGORITHM FOR BRAIN MR IMAGE SEGMENTATION METHOD

Entropy has first introduced in thermodynamics developing an information theoretical concept which is closely connected to the internal energy of the system. It has significant application in physics, information theory, mathematics and other branches of science and engineering [33]. Entropy is the measure of degree of uncertainty that can be used to characterize the texture of the input image.

Entropy is formulated as follows [34]:

$$-\sum p_i \times \log p_i \tag{2.1}$$

where p_i is the probability of a given symbol.

There are different kinds of entropies with significant applications. Now, some of them are discussed in the following:

a) Shannon entropy:

Shannon entropy provides an absolute limit on the best possible lossless compression of a signal under constraint. Shannon entropy is denoted by $H_s(P_{m1\,m2})$ and defined as

$$H_s(P_{m1\,m2}) = -\sum_{m1}\sum_{m2} p_{m1\,m2} \log p_{m1\,m2} \tag{2.2}$$

where p_{m1}, p_{m2} are probability density functions in 2-D random variable [35].

b) Renyi entropy:

It generalizes the Shannon entropy. This entropy is also important in quantum information where it can be used as a measure of entanglement. It is defined as the entropy of the order of α, where $\alpha \geq 0$ and $\alpha \neq 1$, is constructed as

$$H_r(p_{m1\,m2}) = \frac{1}{1-\alpha} \log \sum_{m1} \sum_{m2} (p_{m1\,m2})^{\alpha} \quad (2.3)$$

Sadek et al. [36] suggested an efficient and fast entropy based method for noisy cell image segmentation based on generalized α - entropy by measuring the maximum structural information of image and locating the optimal threshold desired by segmentation. They mentioned that chief advantages of their proposed method are its high rapidity and its tolerance to presence of noise in the image.

c) Harvrda – Charvel:

This entropy is used for statistical physics and modified by Dracozy. This can be defined as the function of α and can be represented as the following mathematical form

$$H_{hc}\,(p_{m1\,m2}) = \frac{1}{2^{\alpha-1}} \sum_{m1} \sum_{m2} p^{\alpha}_{m1\,m2} - 1 \quad (2.4)$$

d) Kapur entropy:

This entropy is denoted by $H_k(p_{m1\,m2})$ of order of α and type β, is represented as [37]:

$$H_k(p_{m1\,m2}) = \left(\frac{\sum_{m1} \sum_{m2} p^{\alpha+\beta-1}_{m1,\ m2}}{\sum_{m1} \sum_{m2} p^{\beta}_{m1,\ m2}} \right) (2^{1-\alpha} - 1)^{-1} \quad (2.5)$$

e) Vajda entropy:

It is special case of Kapur entropy where β = 1 is taken and Vajda measures $H_v(p_{m1\,m2})$, it is preferred over Kapur's entropy as its calculations are faster and is defined as:

$$H_v(p_{m1,\ m2}) = \left(\frac{\sum_{m1} \sum_{m2} p^{\alpha}_{m1,\ m2}}{\sum_{m1} \sum_{m2} p_{m1,\ m2}} - 1 \right) (2^{1-\alpha} -\ \ 1)^{-1} \quad (2.6)$$

As MR images are sensitive to noise [9] and intensity inhomogeneity, it is very difficult to achieve effective result. So, to detect diseased regions in MR images, it is necessary to segment the image into different tissue regions (CSF, GM, WM) accurately. To improve the robustness of

the conventional FCM algorithm we incorporate Shannon entropy in our proposed method. As entropy is proportional to uncertainty, our goal is to minimize the entropy to obtain better segmented output.

The proposed method allows to partition the image pixels by calculating the centers of clusters, v_i and the membership matrix, U through minimizing the following objective function, J with respect to these cluster centers and membership values in an iterative manner.

$$J = \sum_{i=1}^{C}\sum_{k=1}^{N}\left[\alpha\,\mu_{ik}^{m}\left(1-\ e^{-\frac{\|x_k-v_i\|^2}{2\sigma_i^2}}\right)+\ (1-\ \alpha)p_{ik}^{m}\ e^{-\frac{\|x_k-v_i\|^2}{2\sigma_i^2}}\right] - \sum_{i=1}^{C}\sum_{k=1}^{N} p_{ik}\ \ln(p_{ik})\ - \qquad (2.7)$$

where C is the total number of clusters, N is the number of patterns, α is a parameter (> 0), m is the fuzzifier (> 1) and in our proposed method it is set to 1.75, μ_{ik} is the degree of fuzzy membership of pixel x_k in the i^{th} cluster, $\|*\|$ is any norm expressing the similarity between any measured data and the center, λ_1 is Lagrange multiplier and $-\sum_{i=1}^{C}\sum_{k=1}^{N} p_{ik}\ \ln(p_{ik})$ is the Shannon entropy.

Minimizing the objective function (2.7) with respect to the constraint $\sum_{i=1}^{C}\mu_{ik}=1$, we obtain

$$\frac{\partial}{\partial\mu_{ik}}(J)=0 \qquad (2.8)$$

$$\frac{\partial}{\partial v_i}(J)=0 \qquad (2.9)$$

Differentiating the equation (2.7) partially with respect to μ_{ik}, we get the following equation:

$$\frac{\partial}{\partial\mu_{ik}}(J)=\ \alpha\, m\,\mu_{ik}^{m-1}\left(1-\ e^{-\frac{\|x_k-v_i\|^2}{2\sigma_i^2}}\right)-\ \lambda_1 \qquad (2.10)$$

From equation (2.8) and (2.10), we get

$$\alpha\, m\, \mu_{ik}^{m-1} \left(1 - e^{-\frac{\|x_k - v_i\|^2}{2\sigma_i^2}}\right) - \lambda_1 = 0$$

$$\text{Or, } \mu_{ik} = \left[\frac{\lambda_1}{\alpha\, m \left(1 - e^{-\frac{\|x_k - v_i\|^2}{2\sigma_i^2}}\right)}\right]^{\frac{1}{m-1}} \tag{2.11}$$

Using $\sum_{l=1}^{C} \mu_{lk} = 1$, we get

$$\sum_{l=1}^{C} \left[\frac{\lambda_1}{\alpha\, m \left(1 - e^{-\frac{\|x_k - v_i\|^2}{2\sigma_i^2}}\right)}\right]^{\frac{1}{m-1}} = 1$$

$$\text{Or, } \left[\frac{\lambda_1}{\alpha\, m}\right]^{\frac{1}{m-1}} = \frac{1}{\sum_{l=1}^{C} \left[\frac{1}{\left(1 - e^{-\frac{\|x_k - v_i\|^2}{2\sigma_i^2}}\right)}\right]^{\frac{1}{m-1}}} \tag{2.12}$$

From (2.11) and (2.12), we get

$$\mu_{ik} = \frac{1}{\left[\frac{1 - e^{-\frac{\|x_k - v_i\|^2}{2\sigma_i^2}}}{\sum_{l=1}^{C} \left(1 - e^{-\frac{\|x_k - v_i\|^2}{2\sigma_i^2}}\right)}\right]^{\frac{1}{m-1}}} \tag{2.13}$$

Similarly, deriving equation (2.7) partially with respect to v_i, we get the following equation:

$$\frac{\partial}{\partial v_i}(J) = -\sum_{k=1}^{N} \alpha\, \mu_{ik}^{m}\; e^{-\frac{\|x_k - v_i\|^2}{2\sigma_i^2}}\; \frac{\|x_k - v_i\|}{\sigma_i^2} + \sum_{k=1}^{N}(1-\alpha)\; p_{ik}^{m}\, e^{-\frac{\|x_k - v_i\|^2}{2\sigma_i^2}}\; \frac{\|x_k - v_i\|}{\sigma_i^2} \quad (2.14)$$

From (2.9) and (2.14), we get

$$\sum_{k=1}^{N} [\alpha\; \mu_{ik}^{m} - (1-\alpha)\, p_{ik}^{m}]\, e^{-\frac{\|x_k - v_i\|^2}{2\sigma_i^2}}\; \|x_k - v_i\| = 0$$

$$\text{Or, } v_i = \frac{\sum_{k=1}^{N} [\alpha\; \mu_{ik}^{m} - (1-\alpha)\, p_{ik}^{m}]\; e^{-\frac{\|x_k - v_i\|^2}{2\sigma_i^2}}\; x_k}{\sum_{k=1}^{N} [\alpha\; \mu_{ik}^{m} - (1-\alpha)\, p_{ik}^{m}]\; e^{-\frac{\|x_k - v_i\|^2}{2\sigma_i^2}}} \quad (2.15)$$

We now introduce two different ways to calculate the p_{ik} as follows:

2.a) Method 1: p_{ik} is derived from the objective function (2.7).

2.b) Method 2: p_{ik} is calculated depending on the local neighbourhood of a pixel x_k taken as center.

2.a) Method 1:

For the first case, minimizing the objective function (2.7) with the constraint $\sum_{i=1}^{C} \mu_{ik} = 1$, we obtain

$$\frac{\partial}{\partial p_{ik}}(J) = 0 \quad (2.16)$$

Differentiating equation (2.7) partially with respect to p_{ik}, we get

$$\frac{\partial}{\partial p_{ik}}(J) = (1 - \alpha)\, m\, p_{ik}^{m-1}\; e^{-\frac{\|x_k - v_i\|^2}{2\sigma_i^2}} - \ln(p_{ik}) - 1 \qquad (2.17)$$

From (2.16) and (2.17), we have

$$(1 - \alpha)\, m\, p_{ik}^{m-1}\; e^{-\frac{\|x_k - v_i\|^2}{2\sigma_i^2}} - \ln(p_{ik}) - 1 = 0$$

$$\text{Or, } \ln(p_{ik}) = (1 - \alpha)\, m\, p_{ik}^{m-1}\; e^{-\frac{\|x_k - v_i\|^2}{2\sigma_i^2}} - 1$$

$$p_{ik} = e^{\left[(1-\alpha)\, m\, p_{ik}^{m-1}\; e^{-\frac{\|x_k - v_i\|^2}{2\sigma_i^2}} - 1\right]} \qquad (2.18)$$

This (2.18) is the final expression for p_{ik} derived from the objective function (2.7).

2.b) Method 2:

In the second case, we considered the following expression to calculate the entropy in the local neighbourhood of a pixel x_k taken as center.

$$p_{ik} = \frac{e^{-\frac{\|\overline{x_k} - v_i\|^2}{2\sigma_i^2}}}{\sum_{j=1}^{C} e^{-\frac{\|\overline{x_k} - v_j\|^2}{2\sigma_j^2}}} \qquad (2.19)$$

In the above mentioned equation, $\overline{x_k} = \frac{1}{N_k}\sum_{j=1}^{N_k} x_j$ and N_k is considered as the 3×3 local neighbourhood of a pixel x_k taken as center.

CHAPTER 3
EXPERIMENTAL RESULTS

The performance of the proposed method is evaluated first on the BrainWeb [38], IBSR [39] simulated T1-weighted, next on BrainWeb simulated T2-weighted and later on real-patient MR images of human brain in qualitatively and quantitatively manner both. For comparative study, the FCM, FGFCM [24], sFCM [26], ASIFC [25], PFCM methods are included.
The performance of the proposed method is first examined without varying the receptive field of the Gaussian function and then varying the receptive field of the Gaussian function respectively.

3.1 Without Varying Receptive Field of Gaussian Function:

Here, we consider a suitable value for the receptive field of the Gaussian function in the expression of p_{ik} to get superior result in our proposed method.

3.1.1 Simulated MR brain images:

The BrainWeb simulated T1-weighted and T2-weighted MR images of human brain are obtained from the McConnell Brain Imaging Centre of the Montreal Neurological Institute, McGill University [40]. Ten different combinations of both simulated T1 and T2 data volumes have been gathered where T1-weighted data volumes contain 81 images each and T2-weighted data volumes contain 51 images each. In both the image volumes the CSF, GM and WM regions are well distinguished. The image volumes include the images of the following combinations respectively:
1% noise, 20% inhomogeneity; 1% noise, 40% inhomogeneity; 3% noise, 20% inhomogeneity; 3% noise, 40% inhomogeneity; 5% noise, 20% inhomogeneity; 5% noise, 40% inhomogeneity; 7% noise, 20% inhomogeneity; 7% noise, 40% inhomogeneity; 9% noise, 20% inhomogeneity; 9% noise, 40% inhomogeneity. The image resolutions are 181 x 217 x 181 voxels and sized 1 mm x 1 mm x 1 mm.

3.1.1.1 Qualitative evaluation

Here, we present the qualitative outputs of the proposed method. The qualitative evaluations are very useful on the target application, as these give us the type and quality of the images, the weaknesses of the segmentation algorithm, and the results of the individual steps of a method. This section involves segmentation result of different tissue regions, like cerebrospinal fluid (CSF), grey matter (GM), white matter (WM) and total segmented result of the original MR brain image. The performance of the proposed method has been examined at different combinations of noise and intensity inhomogeneity on the T1-weighted and T2-weighted simulated MR brain image volumes. Fig. 2 shows the qualitative results of segmentation of BrainWeb T1-weighted image (slice 96, Fig. 2(a)), with 9% noise and 40% inhomogeneity. Fig 2(b) - (e) give the segmented regions of the original image, CSF, GM, and WM respectively by method 1. Fig 2(f) – (i) give the segmented regions of the original image, CSF, GM, and WM respectively by method 2. Fig. 3 shows the qualitative results of segmentation of BrainWeb T2-weighted image (slice 100, Fig. 3(a)), with 9% noise and 40% inhomogeneity. Fig 3(b) - (e) give the segmented regions of the original image, CSF, GM, and WM respectively by method 1. Fig 3(f) – (i) give the segmented regions of the original image, CSF, GM, and WM respectively by method 2. Fig. 4 shows the qualitative results of segmentation of IBSR T1-weighted image (slice 149, Fig. 4(a)), volume 5. Fig 4(b) - (e) give the segmented regions of the original image, CSF, GM, and WM respectively by method 1. Fig 4(f) – (i) give the segmented regions of the original image, CSF, GM, and WM respectively by method 2.

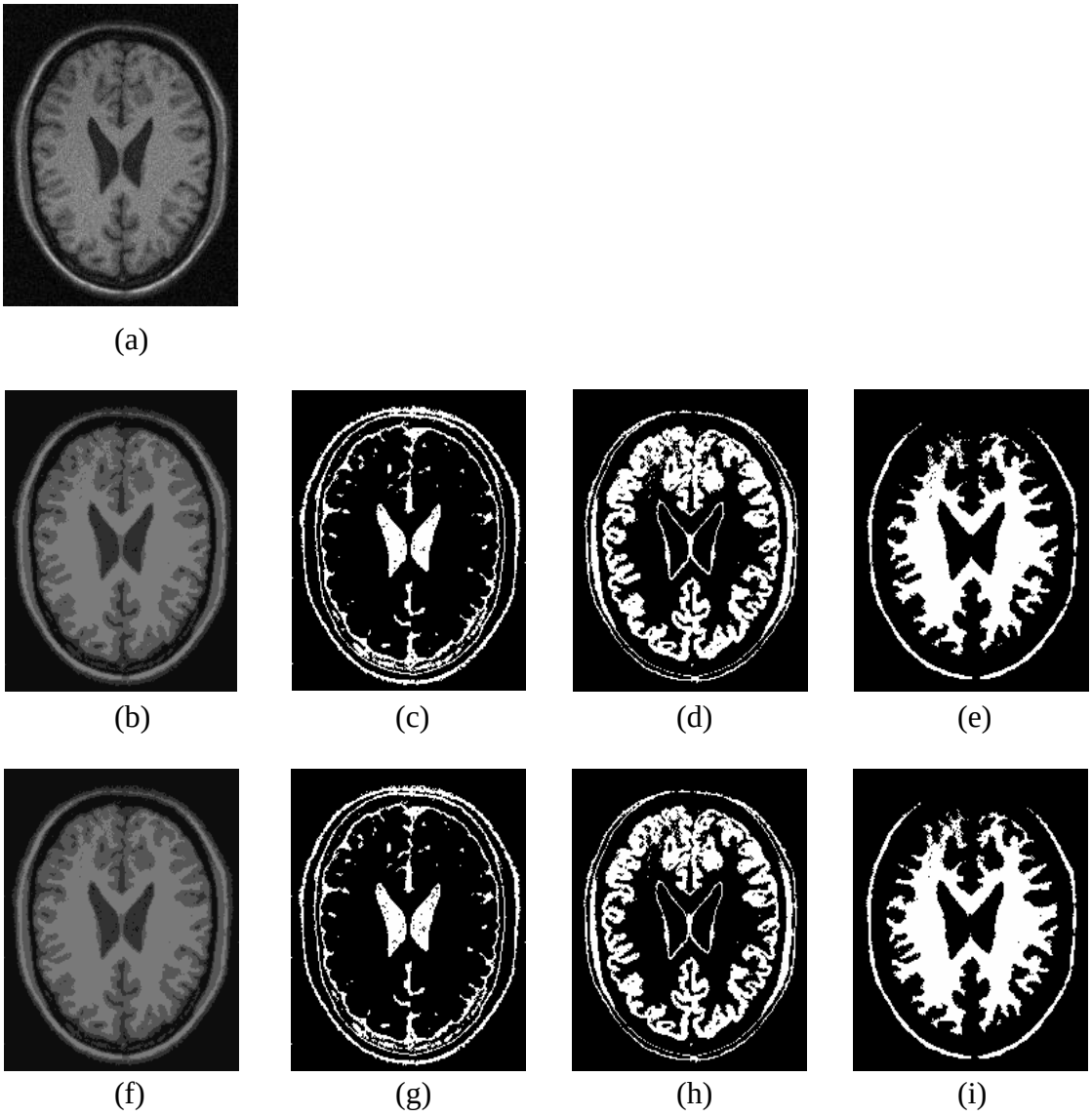

Fig 2: Qualitative segmented results of the original image, CSF, GM, and WM (from left to right) by the proposed methods on BrainWeb T1-weighted MR image with 9% noise and 40% inhomogeneity (a). (b) – (e): method 1; (f) – (i): method 2.

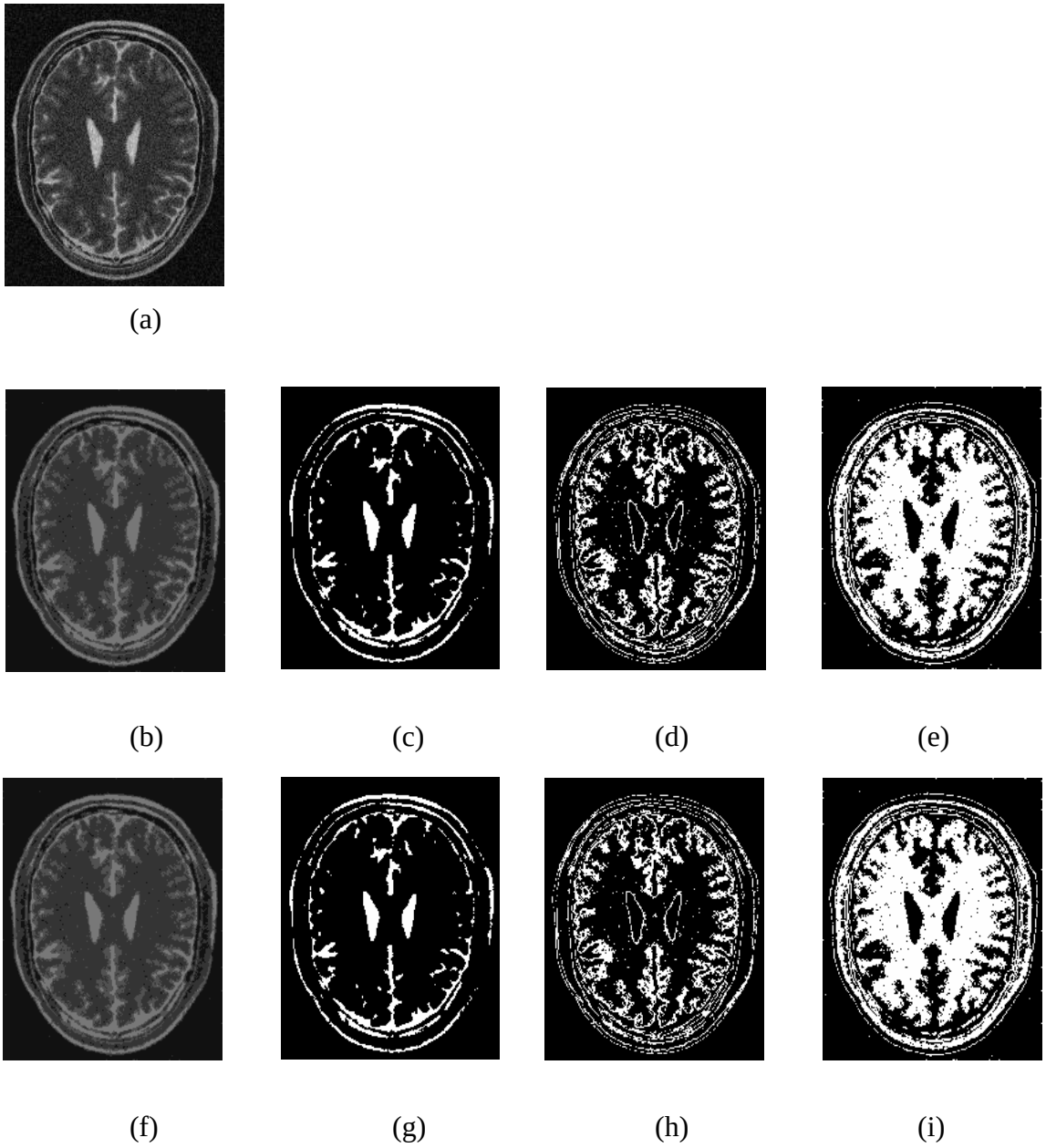

(a)

(b) (c) (d) (e)

(f) (g) (h) (i)

Fig 3: Qualitative segmented results of the original image, CSF, GM, and WM (from left to right) by the proposed methods on BrainWeb T2-weighted MR image with 9% noise and 40% inhomogeneity (a). (b) – (e): method 1; (f) – (i): method 2.

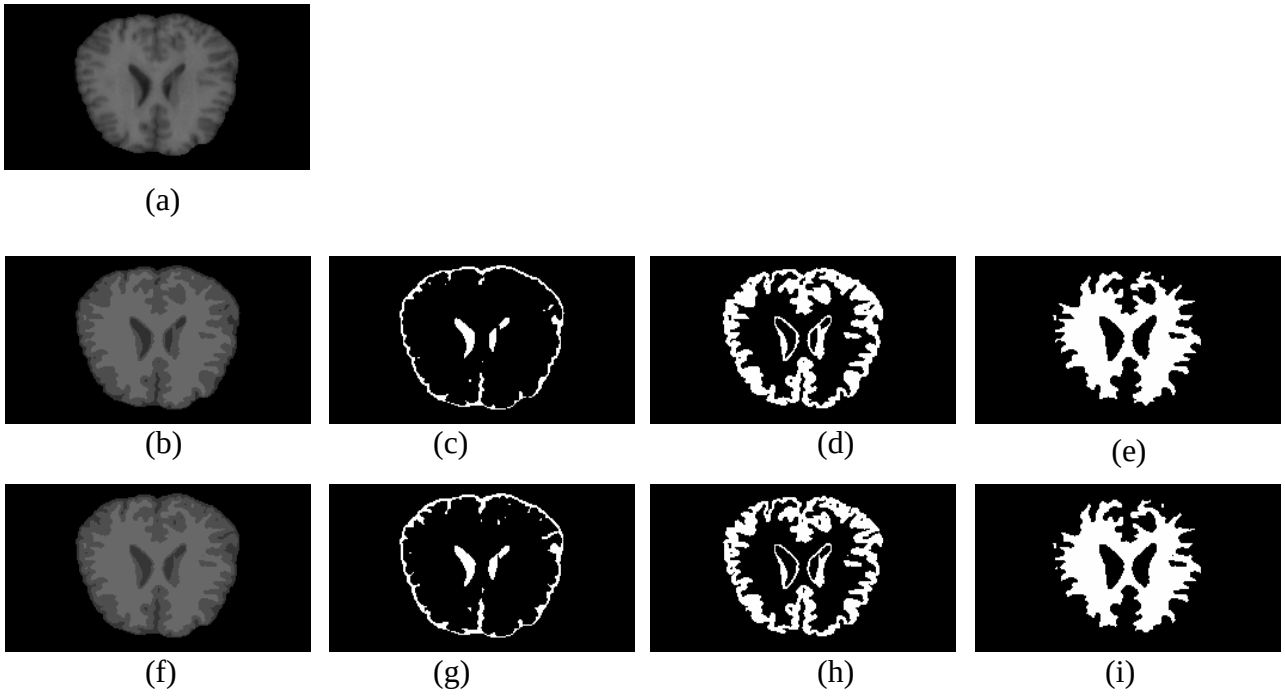

Fig 4: Qualitative segmented results of the original image, CSF, GM, and WM (from left to right) by the proposed methods on IBSR T1-weighted MR image of volume 05 (a). (b) – (e): method 1; (f) – (i): method 2.

3.1.1.2 Quantitative evaluation

For comparative study quantitative evaluation is essential. We have presented three types of quantitative evaluation based on (i) cluster validity functions, (ii) segmentation accuracy and (iii) tissue segmentation accuracy. The cluster validity functions are presented in terms of (i) partition coefficient, (ii) partition entropy and (iii) similarity index. To reduce the influence of the selected images, results are provided as the average values of 81 images (slice 50 – slice 130) from each volume of the simulated T1 weighted MR brain images and 51 images (slice 50 – slice 100) from each volume of the simulated T2-weighted MR brain images.

3.1.1.2.1 Cluster validity functions:

(a) Partition coefficient (V_{pc}): Partition coefficient is one of the most important indicators of fuzzy partition and provides best performance with less fuzziness when the value of V_{pc} takes its optimal value as 1, with higher values being "better". It can be represented as follows [25, 27, 41]:

$$V_{pc} = \frac{\sum_{i=1}^{C} \sum_{k=1}^{N} \mu_{ik}^{2}}{N} \tag{3.1}$$

In Fig. 5 comparative results in terms of V_{pc} for the proposed method 1 and method 2 over 10 BrainWeb T1-weighted MR brain image volumes with different combination of noise and inhomogeneity are shown. In Fig. 6 comparative results in terms of V_{pc} for the proposed method 1 and method 2 over 10 BrainWeb T2-weighted MR brain image volumes with different combination of noise and inhomogeneity are shown. Similarly, in Fig. 7 V_{pc} for the proposed method 1 and method 2 is compared over 3 IBSR T1-weighted MR brain image volumes.

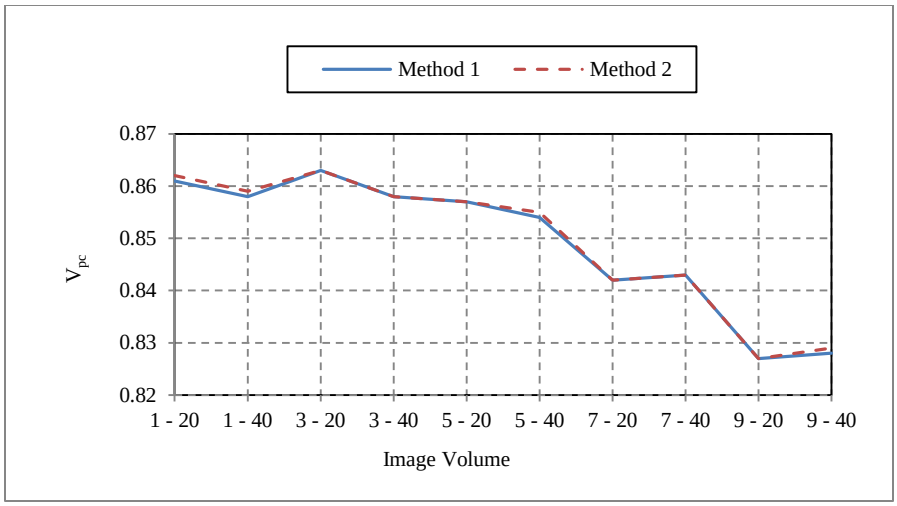

Fig. 5: Comparative study in terms of V_{pc} for the proposed method 1 and method 2 over 10 BrainWeb T1-weighted MR brain image volumes with different combination of noise and inhomogeneity.

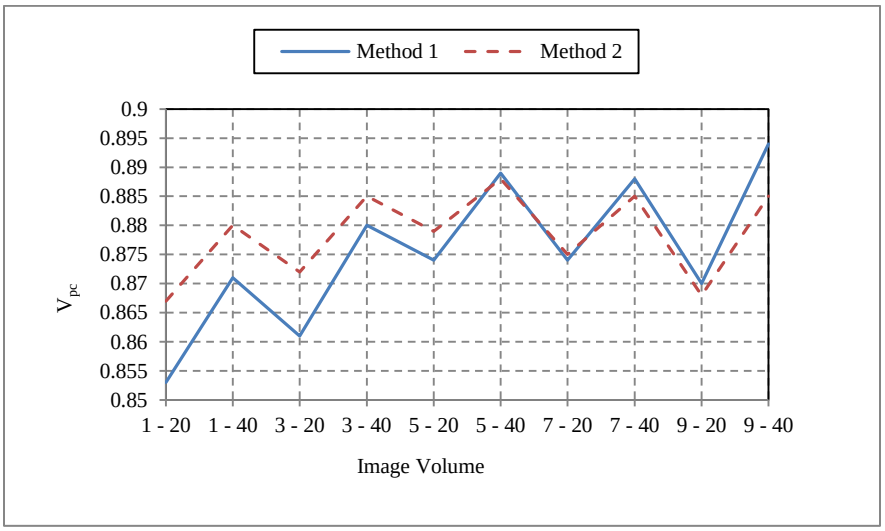

Fig. 6: Comparative study in terms of V_{pc} for the proposed method 1 and method 2 over 10 BrainWeb T2-weighted MR brain image volumes with different combination of noise and inhomogeneity.

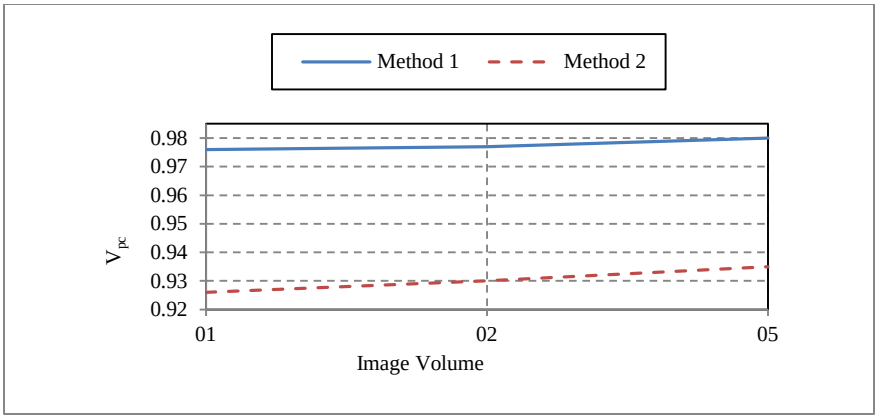

Fig. 7: Comparative study in terms of V_{pc} for the proposed method 1 and method 2 over 3 IBSR T1-weighted MR brain image volumes.

(b) Partition entropy (V_{pe}): Partition entropy is another important indicator of fuzzy partition. To achieve best clustering the value of V_{pe} should be minimal and its value is 0, with lower values being "better". It can be stated as follows [25, 27, 42]:

$$V_{pe} = \frac{-\sum_{i=1}^{C}\sum_{k=1}^{N}[\mu_{ik} \ \log \mu_{ik}]}{N} \tag{3.2}$$

In Fig. 8 comparative results in terms of V_{pe} for the proposed method 1 and method 2 over 10 BrainWeb T1-weighted MR brain image volumes with different combination of noise and inhomogeneity are shown. In Fig. 9 comparative results in terms of V_{pe} for the proposed method 1 and method 2 over 10 BrainWeb T2-weighted MR brain image volumes with different combination of noise and inhomogeneity are shown. Similarly, in Fig. 10 V_{pe} for the proposed method 1 and method 2 is compared over 3 IBSR T1-weighted MR brain image volumes.

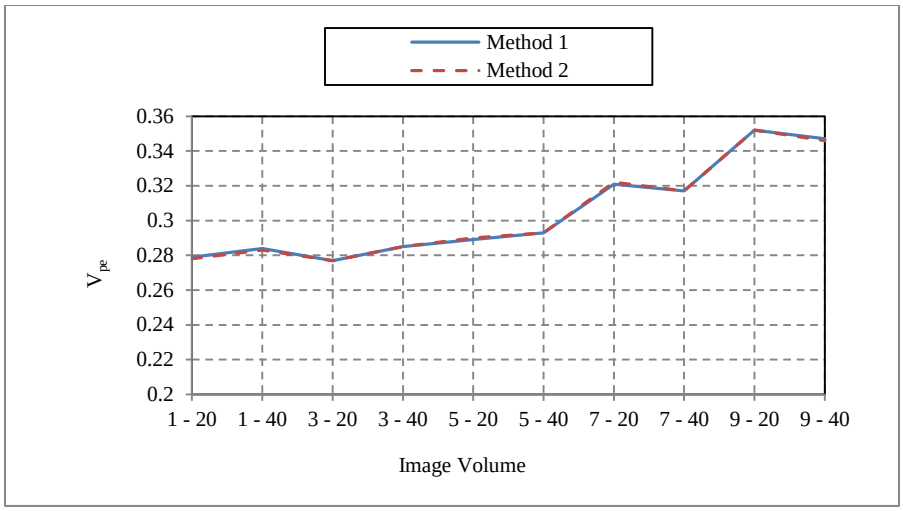

Fig. 8: Comparative study in terms of V_{pe} for the proposed method 1 and method 2 over 10 BrainWeb T1-weighted MR brain image volumes with different combination of noise and inhomogeneity.

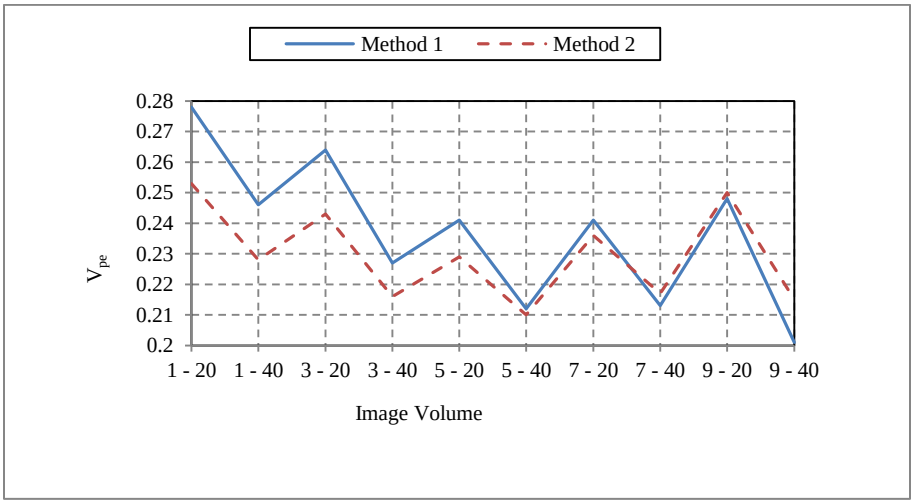

Fig. 9: Comparative study in terms of V_{pe} for the proposed method 1 and method 2 over 10 BrainWeb T2-weighted MR brain image volumes with different combination of noise and inhomogeneity.

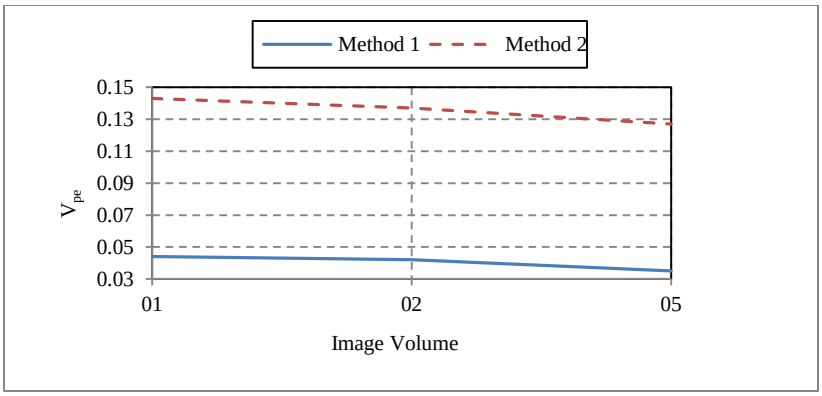

Fig. 10: Comparative study in terms of V_{pe} for the proposed method 1 and method 2 over 3 IBSR T1-weighted MR brain image volumes.

(c) Similarity index (ρ): Let for an image with C clusters, if A_i and B_i represent the sets of pixels belonging to cluster *i* in the segmented image and in "ground truth" image, respectively, then the similarity index $\boldsymbol{\rho}$ is defined as follows [4]:

$$\boldsymbol{\rho} = \frac{1}{C}\sum_{i=1}^{C}\frac{2\ |A_i \cap B_i|}{|A_i\ |+\ |B_i|} \times 100\% \qquad (3.3)$$

The value of similarity index is ranged in [0, 1] and the optimal clustering result is achieved when $\boldsymbol{\rho}$ = 1, with higher value being "better". It is a very efficient validity measurement as it compares the segmentation results with the ground truth. Noise and inhomogeneity free image is considered here as the ground truth image. In Fig. 11 comparative results in terms of $\boldsymbol{\rho}$ for the proposed method 1 and method 2 over 10 BrainWeb T1-weighted MR brain image volumes with different combination of noise and inhomogeneity are shown. In Fig. 12 comparative results in terms of $\boldsymbol{\rho}$ for the proposed method 1 and method 2 over 10 BrainWeb T2-weighted MR brain image volumes with different combination of noise and inhomogeneity are shown. Similarly, in Fig. 13 $\boldsymbol{\rho}$ for the proposed method 1 and method 2 is compared over 3 IBSR T1-weighted MR brain image volumes.

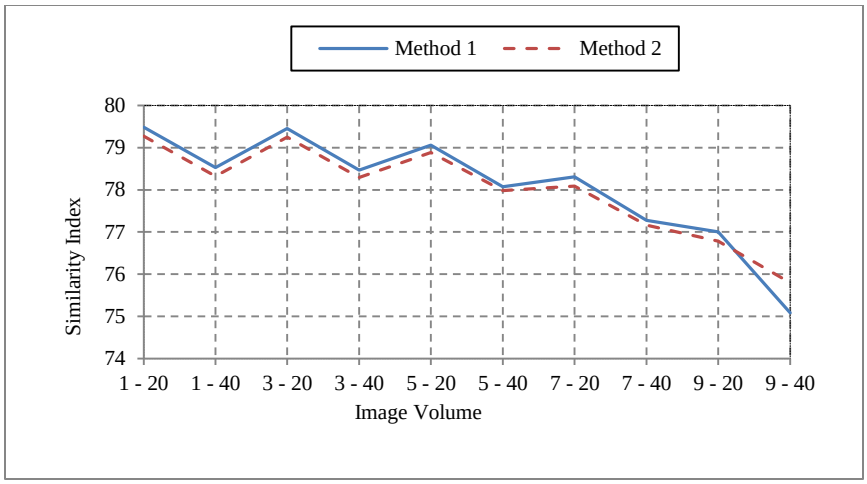

Fig. 11: Comparative study in terms of ρ for the proposed method 1 and method 2 over 10 BrainWeb T1-weighted MR brain image volumes with different combination of noise and inhomogeneity.

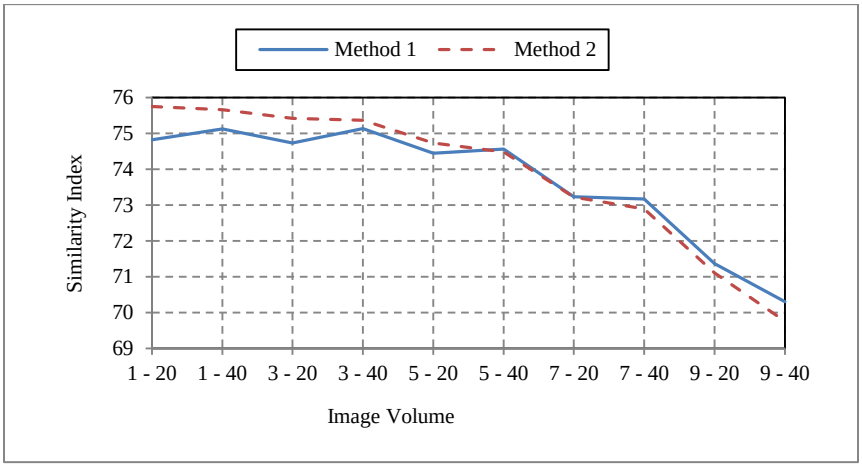

Fig. 12: Comparative study in terms of ρ for the proposed method 1 and method 2 over 10 BrainWeb T2-weighted MR brain image volumes with different combination of noise and inhomogeneity.

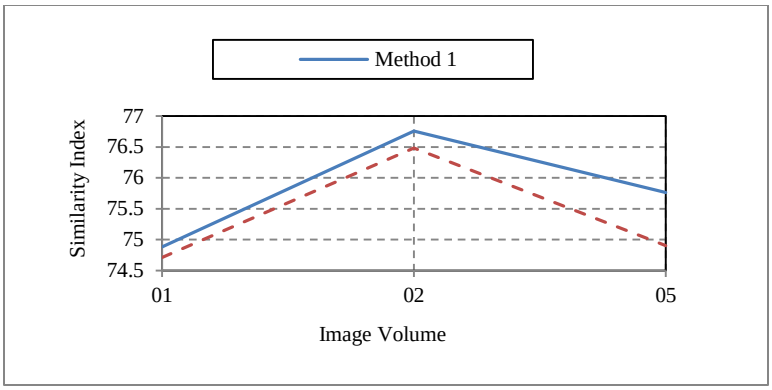

Fig.13: Comparative study in terms of $\boldsymbol{\rho}$ for the proposed method 1 and method 2 over 3 IBSR T1-weighted MR brain image volumes.

3.1.1.2.2. Segmentation accuracy (SA):

The SA is defined as the sum of the correctly classified pixels divided by the sum of the total number of pixels of the clustered image. The SA can be represented as follows [4]:

$$SA = \frac{card(A_j \cap C_j)}{card(C_j)} \tag{3.4}$$

In the above mentioned expression, A_j is the set of pixels belonging to the j^{th} cluster found by the proposed method, C_j is the set of pixels of the j^{th} cluster in the ground truth image. For an ideal result, the value of SA will be 1, with higher values being "better". Table 1 describes the comparative performance of different segmentation algorithms in terms of segmentation accuracy on the 10 BrainWeb T1-weighted MR brain image volumes with different combination of noise and intensity inhomogeneity. Table 2 describes the comparative performance of different segmentation algorithms in terms of segmentation accuracy on the 3 IBSR T1-weighted MR brain image volumes. Similarly, in Table 3 the comparative performance of proposed methods in terms of segmentation accuracy on the 10 BrainWeb T2-weighted MR brain image volumes with different combination of noise and intensity inhomogeneity is shown.

Table 1:
Comparative performance of different segmentation algorithms in terms of segmentation accuracy on the BrainWeb T1-weighted MR brain image volumes with different combination of noise and intensity inhomogeneity.

Volumes (Noise% - IIH%)	Tissue Regions	Segmentation Accuracy (SA)								
		FCM	FGFCM	sFCM	ASIFC	PFCM	Method 1	Standard deviation	Method 2	Standard deviation
1 – 20	CSF	0.956	0.938	0.966	0.969	0.961	0.925	±0.016	0.924	±0.014
	GM	0.922	0.895	0.938	0.942	0.935	0.941	±0.012	0.929	±0.014
	WM	0.966	0.977	0.975	0.978	0.976	0.972	±0.009	0.980	±0.004
1 – 40	CSF	0.938	0.917	0.944	0.947	0.950	0.926	±0.016	0.924	±0.013
	GM	0.874	0.853	0.931	0.934	0.875	0.927	±0.016	0.912	±0.018
	WM	0.918	0.959	0.968	0.973	0.940	0.940	±0.009	0.953	±0.007
3 – 20	CSF	0.930	0.906	0.938	0.942	0.949	0.928	±0.015	0.928	±0.012
	GM	0.865	0.848	0.927	0.931	0.907	0.936	±0.013	0.922	±0.014
	WM	0.907	0.951	0.956	0.960	0.974	0.966	±0.012	0.977	±0.004
3 – 40	CSF	0.910	0.893	0.921	0.926	0.925	0.927	±0.014	0.925	±0.012
	GM	0.849	0.835	0.922	0.924	0.850	0.923	±0.016	0.906	±0.017
	WM	0.898	0.944	0.947	0.952	0.937	0.934	±0.012	0.950	±0.007
5 – 20	CSF	0.881	0.861	0.907	0.911	0.907	0.921	±0.014	0.919	±0.014
	GM	0.834	0.828	0.916	0.919	0.879	0.927	±0.013	0.910	±0.013
	WM	0.848	0.941	0.938	0.946	0.959	0.955	±0.019	0.971	±0.004
5 – 40	CSF	0.837	0.832	0.861	0.867	0.875	0.919	±0.015	0.915	±0.015
	GM	0.825	0.821	0.909	0.911	0.837	0.914	±0.017	0.896	±0.015
	WM	0.840	0.916	0.926	0.933	0.925	0.920	±0.021	0.945	±0.007
7 – 20	CSF	0.819	0.816	0.852	0.859	0.836	0.902	±0.018	0.897	±0.018
	GM	0.818	0.801	0.902	0.907	0.815	0.910	±0.015	0.891	±0.013
	WM	0.829	0.909	0.912	0.918	0.949	0.943	±0.023	0.963	±0.006
7 – 40	CSF	0.807	0.795	0.849	0.852	0.817	0.901	±0.019	0.893	±0.019
	GM	0.782	0.792	0.895	0.989	0.772	0.901	±0.020	0.879	±0.016
	WM	0.795	0.906	0.903	0.908	0.926	0.902	±0.029	0.935	±0.007
9 – 20	CSF	0.753	0.739	0.827	0.836	0.777	0.870	±0.025	0.856	±0.018
	GM	0.755	0.736	0.871	0.875	0.762	0.892	±0.020	0.868	±0.015
	WM	0.781	0.873	0.897	0.901	0.932	0.918	±0.037	0.950	±0.010
9 - 40	CSF	0.742	0.731	0.824	0.829	0.753	0.868	±0.029	0.851	±0.019
	GM	0.742	0.725	0.862	0.868	0.737	0.879	±0.022	0.855	±0.016
	WM	0.765	0.876	0.873	0.880	0.914	0.842	±0.172	0.921	±0.009

Table 2:
Comparative performance of different segmentation algorithms in terms of segmentation accuracy on the IBSR T1-weighted MR brain image volumes.

Volumes	Tissue Regions	Segmentation Accuracy (SA)								
		FCM	FGFCM	sFCM	ASIFC	PFCM	Method 1	Standard deviation	Method 2	Standard deviation
Vol 1	CSF	0.767	0.752	0.832	0.837	0.726	0.846	±0.052	0.901	±0.047
	GM	0.629	0.613	0.693	0.696	0.620	0.672	±0.059	0.678	±0.049
	WM	0.950	0.948	0.947	0.958	0.955	0.889	±0.020	0.891	±0.026
Vol 2	CSF	0.756	0.745	0.778	0.782	0.737	0.801	±0.124	0.831	±0.113
	GM	0.748	0.729	0.786	0.793	0.732	0.768	±0.064	0.756	±0.059
	WM	0.944	0.951	0.949	0.956	0.954	0.909	±0.013	0.906	±0.014
Vol 5	CSF	0.623	0.611	0.631	0.636	0.611	0.716	±0.075	0.793	±0.063
	GM	0.753	0.749	0.827	0.831	0.799	0.751	±0.058	0.718	±0.051
	WM	0.632	0.758	0.753	0.778	0.775	0.921	±0.017	0.909	±0.019

Table 3:
Comparative performance of proposed algorithms in terms of segmentation accuracy on the BrainWeb T2-weighted MR brain image volumes with different combination of noise and intensity inhomogeneity.

Volumes (Noise% - IIH%)	Tissue Regions	Segmentation Accuracy (SA)			
		Method 1	Standard deviation	Method 2	Standard deviation
1 – 20	CSF	0.986	±0.014	0.994	±0.002
	GM	0.796	±0.015	0.813	±0.015
	WM	0.954	±0.022	0.962	±0.022
1 – 40	CSF	0.988	±0.006	0.989	±0.003
	GM	0.802	±0.022	0.807	±0.023
	WM	0.935	±0.032	0.944	±0.031
3 – 20	CSF	0.994	±0.002	0.992	±0.003
	GM	0.791	±0.016	0.800	±0.016
	WM	0.943	±0.028	0.954	±0.026
3 – 40	CSF	0.987	±0.004	0.985	±0.004
	GM	0.794	±0.022	0.787	±0.025
	WM	0.934	±0.032	0.945	±0.029
5 – 20	CSF	0.989	±0.003	0.986	±0.004
	GM	0.775	±0.018	0.765	±0.021
	WM	0.934	±0.027	0.949	±0.023
5 – 40	CSF	0.978	±0.007	0.974	±0.006
	GM	0.759	±0.024	0.739	±0.027
	WM	0.935	±0.025	0.948	±0.021
7 – 20	CSF	0.982	±0.005	0.976	±0.005
	GM	0.729	±0.013	0.705	±0.013
	WM	0.922	±0.021	0.941	±0.016
7 – 40	CSF	0.965	±0.011	0.961	±0.011
	GM	0.700	±0.015	0.674	±0.018
	WM	0.931	±0.016	0.944	±0.013
9 – 20	CSF	0.967	±0.009	0.961	±0.009
	GM	0.669	±0.014	0.639	±0.020
	WM	0.901	±0.014	0.916	±0.012
9 - 40	CSF	0.913	±0.033	0.909	±0.035
	GM	0.573	±0.060	0.548	±0.065
	WM	0.931	±0.011	0.932	±0.013

3.1.1.2.3. Tissue segmentation accuracy (TSA):

The TSA is defined as follows [4]:

$$TSA = \frac{2N_{CTK}}{N_{CITK} + N_{GTK}} \tag{3.5}$$

In the above definition, N_{CTK} denotes the number of pixels that are correctly assigned to tissue *k* by a the proposed method. N_{CITK} is the total number of pixels assigned to tissue *k* and N_{GTK} is the number of pixels belonging to the tissue *k* in the ground truth. For an ideal result, TSA will be 1, with higher values being "better". Table 4 describes the comparative performance of different segmentation algorithms in terms of tissue segmentation accuracy on the 10 BrainWeb T1-weighted MR brain image volumes with different combination of noise and intensity inhomogeneity. Table 5 describes the comparative performance of different segmentation algorithms in terms of tissue segmentation accuracy on the 3 IBSR T1-weighted MR brain image volumes. Similarly, in Table 6 the comparative performance of proposed methods in terms of tissue segmentation accuracy on the 10 BrainWeb T2-weighted MR brain image volumes with different combination of noise and intensity inhomogeneity is shown.

Table 4:
Comparative performance of different segmentation algorithms in terms of tissue segmentation accuracy on the BrainWeb T1-weighted MR brain image volumes with different combination of noise and intensity inhomogeneity.

Volumes (Noise% - IIH%)	Tissue Regions	Tissue Segmentation Accuracy (TSA)								
		FCM	FGFCM	sFCM	ASIFC	PFCM	Method 1	Standard deviation	Method 2	Standard deviation
1 – 20	CSF	0.463	0.465	0.652	0.668	0.452	0.569	±0.046	0.571	±0.049
	GM	0.724	0.720	0.845	0.862	0.720	0.829	±0.017	0.826	±0.017
	WM	0.741	0.738	0.853	0.873	0.741	0.865	±0.055	0.859	±0.060
1 – 40	CSF	0.458	0.462	0.645	0.657	0,427	0.565	±0.046	0.568	±0.050
	GM	0.719	0.715	0.837	0.848	0.691	0.811	±0.017	0.807	±0.018
	WM	0.738	0.731	0.851	0.862	0.729	0.851	±0.050	0.846	±0.057
3 – 20	CSF	0.451	0.458	0.633	0.642	0.451	0.578	±0.046	0.581	±0.049
	GM	0.717	0.711	0.831	0.843	0.710	0.828	±0.017	0.824	±0.017
	WM	0.735	0.731	0.847	0.858	0.730	0.863	±0.055	0.857	±0.060
3 – 40	CSF	0.442	0.447	0.623	0.639	0.424	0.573	±0.047	0.576	±0.049
	GM	0.698	0.691	0.825	0.836	0.684	0.810	±0.017	0.806	±0.017
	WM	0.724	0.719	0.842	0.854	0.720	0.850	±0.051	0.845	±0.057
5 – 20	CSF	0.439	0.442	0.615	0.623	0.494	0.580	±0.048	0.584	±0.050
	GM	0.693	0.689	0.817	0.829	0.690	0.823	±0.016	0.820	±0.016
	WM	0.716	0.714	0.839	0.846	0.717	0.857	±0.057	0.853	±0.061
5 – 40	CSF	0.419	0.426	0.609	0.618	0.414	0.575	±0.050	0.579	±0.051
	GM	0.678	0.673	0.811	0.825	0.672	0.806	±0.016	0.805	±0.016
	WM	0.714	0.712	0.831	0.842	0.711	0.845	±0.054	0.842	±0.057
7 – 20	CSF	0.417	0.421	0.602	0.611	0.418	0.576	±0.051	0.579	±0.052
	GM	0.660	0.654	0.795	0.816	0.651	0.813	±0.015	0.810	±0.016
	WM	0.694	0.691	0.822	0.835	0.690	0.850	±0.059	0.844	±0.064
7 – 40	CSF	0.390	0.392	0.592	0.601	0.397	0.568	±0.052	0.572	±0.052
	GM	0.645	0.637	0.778	0.792	0.629	0.795	±0.017	0.794	±0.017
	WM	0.693	0.689	0.815	0.829	0.684	0.837	±0.056	0.835	±0.059
9 – 20	CSF	0.377	0.381	0.558	0.579	0.366	0.559	±0.054	0.561	±0.050
	GM	0.621	0.613	0.762	0.786	0.605	0.799	±0.016	0.797	±0.016
	WM	0.666	0.664	0.808	0.824	0.660	0.837	±0.063	0.834	±0.065
9 - 40	CSF	0.361	0.372	0.552	0.571	0.358	0.548	±0.057	0.552	±0.051
	GM	0.610	0.605	0.751	0.769	0.590	0.776	±0.022	0.781	±0.016
	WM	0.671	0.670	0.792	0.817	0.662	0.799	±0.160	0.825	±0.062

Table 5:
Comparative performance of different segmentation algorithms in terms of tissue segmentation accuracy on the IBSR T1-weighted MR brain image volumes.

Volumes	Tissue Regions	Tissue Segmentation Accuracy (TSA)								
		FCM	FGFCM	sFCM	ASIFC	PFCM	Method 1	Standard deviation	Method 2	Standard deviation
Vol 1	CSF	0.534	0.537	0.601	0.620	0.633	0.359	±0.092	0.354	±0.093
	GM	0.622	0.619	0.412	0.738	0.608	0.765	±0.042	0.770	±0.036
	WM	0.664	0.657	0.476	0.779	0.650	0.854	±0.042	0.876	±0.046
Vol 2	CSF	0.630	0.633	0.711	0.731	0.629	0.366	±0.086	0.362	±0.083
	GM	0.651	0.642	0.724	0.758	0.640	0.822	±0.036	0.814	±0.033
	WM	0.707	0.689	0.721	0.740	0.701	0.893	±0.044	0.894	±0.043
Vol 5	CSF	0.528	0.538	0.543	0.562	0.569	0.346	±0.053	0.333	±0.053
	GM	0.646	0.632	0.710	0.731	0.733	0.814	±0.038	0.792	±0.033
	WM	0.621	0.618	0.653	0.689	0.681	0.884	±0.054	0.884	±0.053

Table 6:
Comparative performance of proposed algorithms in terms of tissue segmentation accuracy on the BrainWeb T2-weighted MR brain image volumes with different combination of noise and intensity inhomogeneity.

Volumes (Noise% - IIH%)	Tissue Regions	Tissue Segmentation Accuracy (TSA)			
		Method 1	Standard deviation	Method 2	Standard deviation
1 – 20	CSF	0.573	±0.029	0.604	±0.032
	GM	0.781	±0.017	0.788	±0.019
	WM	0.706	±0.113	0.704	±0.111
1 – 40	CSF	0.617	±0.029	0.638	±0.031
	GM	0.773	±0.018	0.775	±0.020
	WM	0.684	±0.115	0.684	±0.113
3 – 20	CSF	0.591	±0.030	0.617	±0.033
	GM	0.771	±0.017	0.775	±0.019
	WM	0.702	±0.113	0.700	±0.111
3 – 40	CSF	0.638	±0.028	0.652	±0.030
	GM	0.763	±0.019	0.761	±0.022
	WM	0.684	±0.113	0.682	±0.111
5 – 20	CSF	0.623	±0.031	0.642	±0.033
	GM	0.750	±0.020	0.747	±0.023
	WM	0.687	±0.112	0.684	±0.110
5 – 40	CSF	0.663	±0.027	0.673	±0.027
	GM	0.736	±0.022	0.728	±0.025
	WM	0.671	±0.111	0.668	±0.109
7 – 20	CSF	0.643	±0.030	0.658	±0.029
	GM	0.713	±0.020	0.704	±0.020
	WM	0.663	±0.114	0.659	±0.114
7 – 40	CSF	0.680	±0.027	0.688	±0.027
	GM	0.694	±0.018	0.681	±0.019
	WM	0.649	±0.114	0.645	±0.116
9 – 20	CSF	0.661	±0.028	0.673	±0.028
	GM	0.666	±0.017	0.651	±0.017
	WM	0.631	±0.115	0.627	±0.118
9 - 40	CSF	0.722	±0.028	0.724	±0.027
	GM	0.601	±0.042	0.585	±0.048
	WM	0.605	±0.130	0.600	±0.132

3.1.2 Real-patient MR images:

We have examined the performance of the proposed method on an image volume consisting of 51 real-patient MR image data, which are collected from the Advanced Medical Research Institute (AMRI) Hospital, Kolkata, India. As the ground truth of segmentation for real-patient MR images is not usually available, thereby the performance of the proposed method on the real-patient MR data is evaluated first qualitatively and later quantitatively in terms of cluster validity functions.

3.1.2.1. Qualitative evaluation

Fig. 14 shows the qualitative results of segmentation of T1-weighted real-patient MR brain image (Fig. 14(a)) by the proposed methods. Fig. 14(b)-(e) show the segmented regions of the original image, CSF, GM, and WM, respectively by the proposed method 1; Fig. 14(f)-(i) show the segmented regions of the original image, CSF, GM, and WM, respectively by the proposed method 2. Fig. 15 shows the qualitative results of segmentation of T2-weighted real-patient MR brain image (Fig. 15(a)) by the proposed methods. Fig. 15(b)-(e) show the segmented regions of the original image, CSF, GM, and WM, respectively by the proposed method 1; Fig. 15(f)-(i) show the segmented regions of the original image, CSF, GM, and WM, respectively by the proposed method 2.

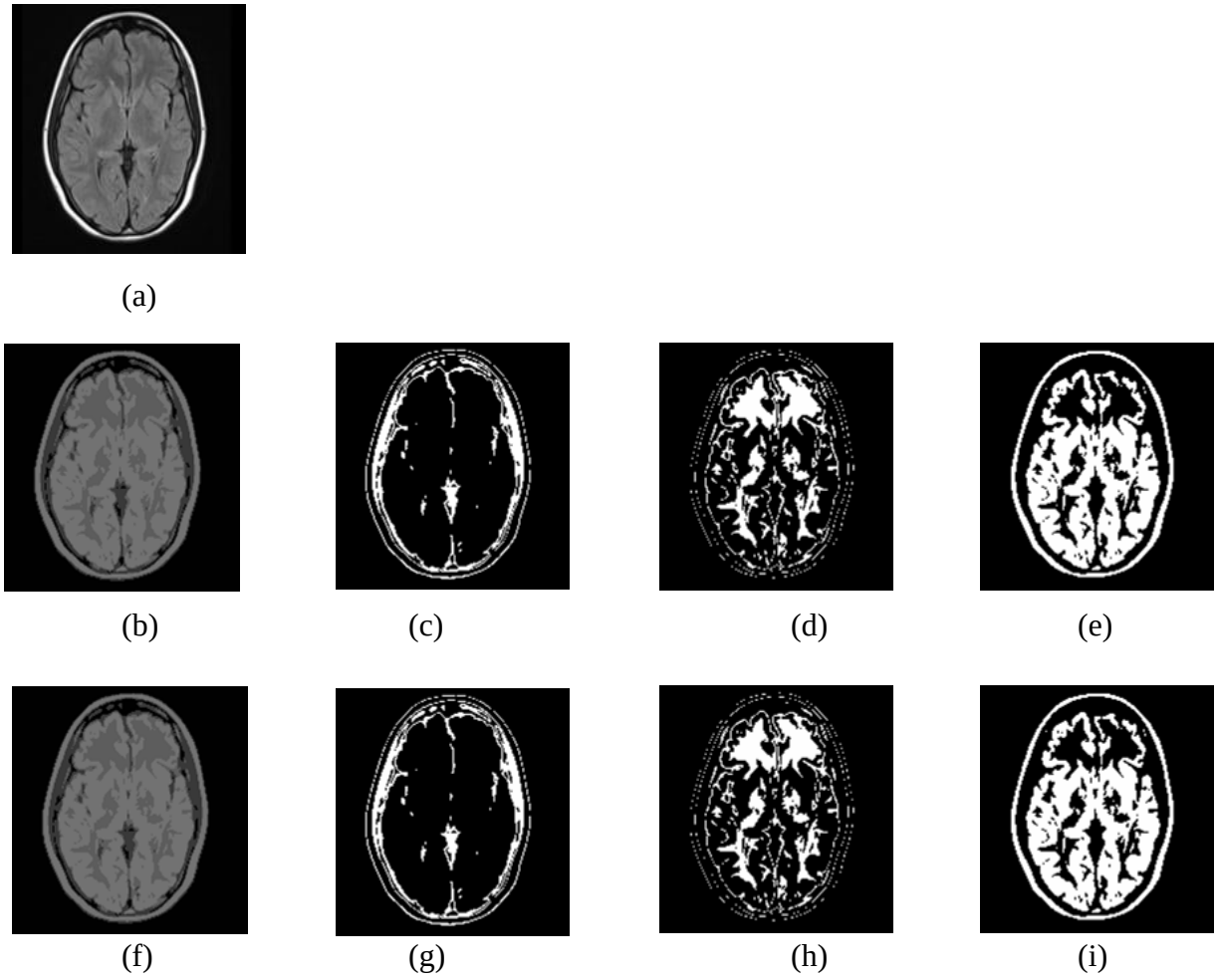

(a)

(b) (c) (d) (e)

(f) (g) (h) (i)

Fig. 14: Qualitative segmented results of the original image, CSF, GM, and WM (from left to right) by the proposed methods on T1-weighted real patient MR image (a). (b) – (e): method 1; (f) – (i): method 2.

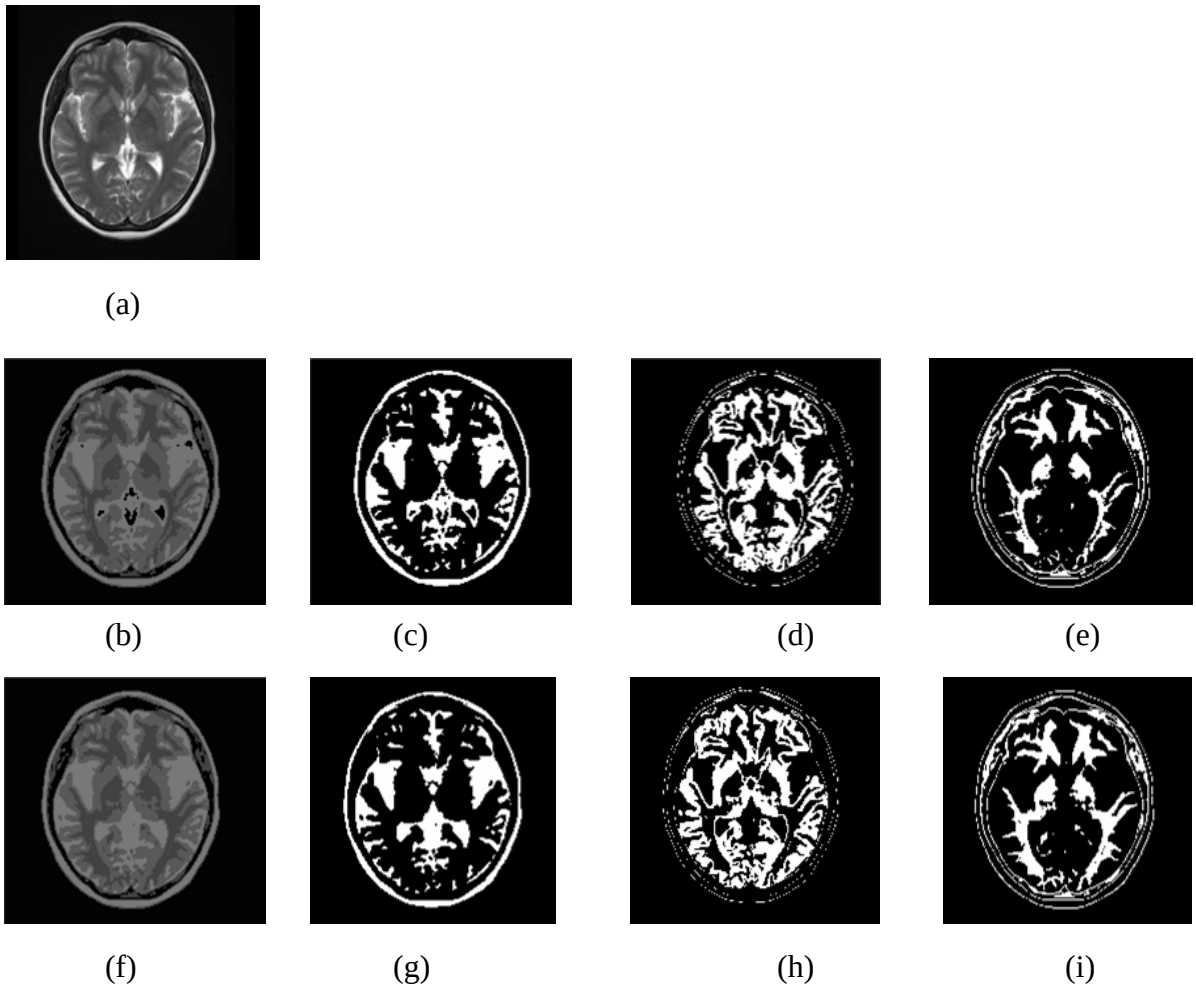

Fig. 15: Qualitative segmented results of the original image, CSF, GM, and WM (from left to right) by the proposed methods onT2-weighted real patient MR image (a). (b) – (e): method 1; (f) – (i): method 2.

3.1.2.2. Quantitative evaluation

Table 7 shows the average V_{pc} and V_{pe} values from the three T1-weighted real-patient MR brain image volumes for the method 1 and method 2. Fig. 16 and Fig. 17 show the average V_{pc} and V_{pe} values from the three T2-weighted real-patient MR brain image volumes for the method 1 and method 2.

Table 7:

Comparative study for different segmentation algorithms of V_{pc} and V_{pe} on three T1-weighted real patient volumes.

Volume	Method	V_{pc}	Standard deviation	V_{pe}	Standard deviation
Real patient 1	FCM	0.791		0.253	
	FGFCM	0.811		0.159	
	sFCM	0.835		0.074	
	ASIFC	0.897		0.056	
	PFCM	0.905		0.053	
	Method 1	0.912	±0.015	0.191	±0.027
	Method 2	0.909	±0.019	0.195	±0.034
Real patient 2	FCM	0.870		0.273	
	FGFCM	0.893		0.193	
	sFCM	0.907		0.178	
	ASIFC	0.922		0.143	
	PFCM	0.935		0.112	
	Method 1	0.901	±0.008	0.211	±0.019
	Method 2	0.917	±0.018	0.175	±0.039
Real patient 3	FCM	0.705		0.558	
	FGFCM	0.815		0.329	
	sFCM	0.886		0.294	
	ASIFC	0.911		0.206	
	PFCM	0.924		0.137	
	Method 1	0.907	±0.012	0.190	±0.024
	Method 2	0.913	±0.012	0.180	±0.023

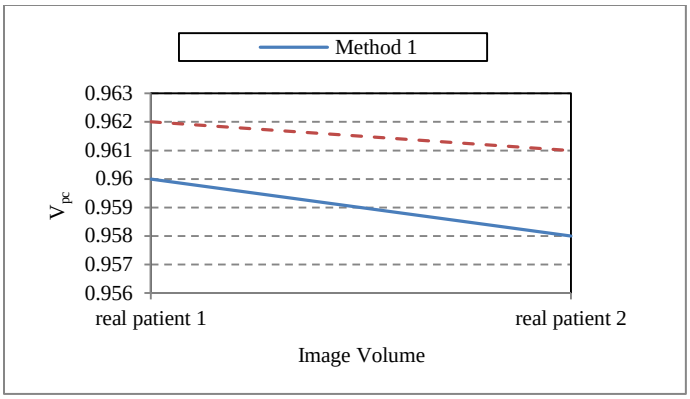

Fig. 16: Comparative study for the two proposed algorithms of V_{pc} on three T2-weighted real patient volumes.

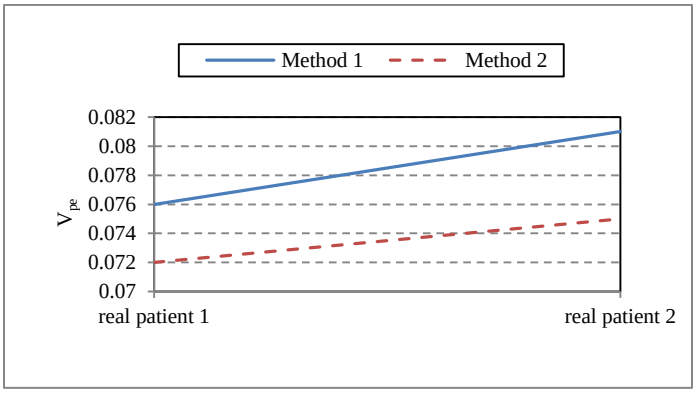

Fig. 17: Comparative study for the two proposed algorithms of V_{pe} on three T2-weighted real patient volumes.

3.2: Varying Receptive Field of the Gaussian Function:

Entropy is involved as the dissimilarity among the pixels in the regions along the edges is very high. So, to calculate the entropy in a local neighbourhood, a threshold value is empirically determined for the expression p_{ik} . If the variance among the pixels in a 5×5 neighbourhood is greater than the threshold, then we take the receptive field 40 times than the original one. Otherwise, it remains the same.

The performance of the proposed method is examined on the same above mentioned databases.

3.2.1. Simulated MR brain images:

3.2.1.1 Qualitative evaluation:

Here, we present the qualitative outputs of the modified proposed method. The performance of the modified proposed method has been examined at different combinations of noise and intensity inhomogeneity on the T1-weighted simulated MR brain image volumes. Fig. 18 shows the qualitative results of segmentation of BrainWeb T1-weighted image (slice 96, Fig. 18(a)), with 9% noise and 40% inhomogeneity. Fig 18(b) - (e) give the segmented regions of the original image, CSF, GM, and WM respectively by method 1 modified. Fig 18(f) – (i) give the segmented regions of the original image, CSF, GM, and WM respectively by method 2 modified. Fig. 19 shows the qualitative results of segmentation of IBSR T1-weighted image (slice 149, Fig. 19(a)), volume 5. Fig 19(b) - (e) give the segmented regions of the original image, CSF, GM, and WM respectively by method 1 modified. Fig 19(f) – (i) give the segmented regions of the original image, CSF, GM, and WM respectively by method 2 modified.

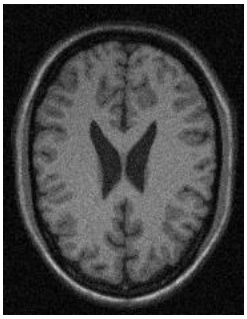

(a)

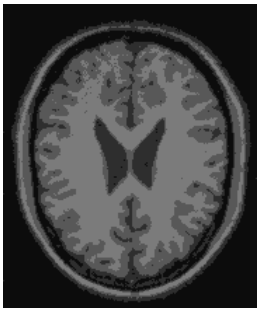

(b)

(c)

(d)

(e)

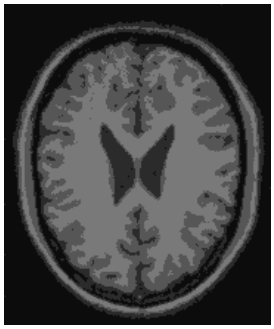

(f)

(g)

(h)

(i)

Fig. 18: Qualitative segmented results of the original image, CSF, GM, and WM (from left to right) by the proposed methods on BrainWeb T1-weighted MR image with 9% noise and 40% inhomogeneity (a). (b) – (e): method 1 modified; (f) – (i): method 2 modified.

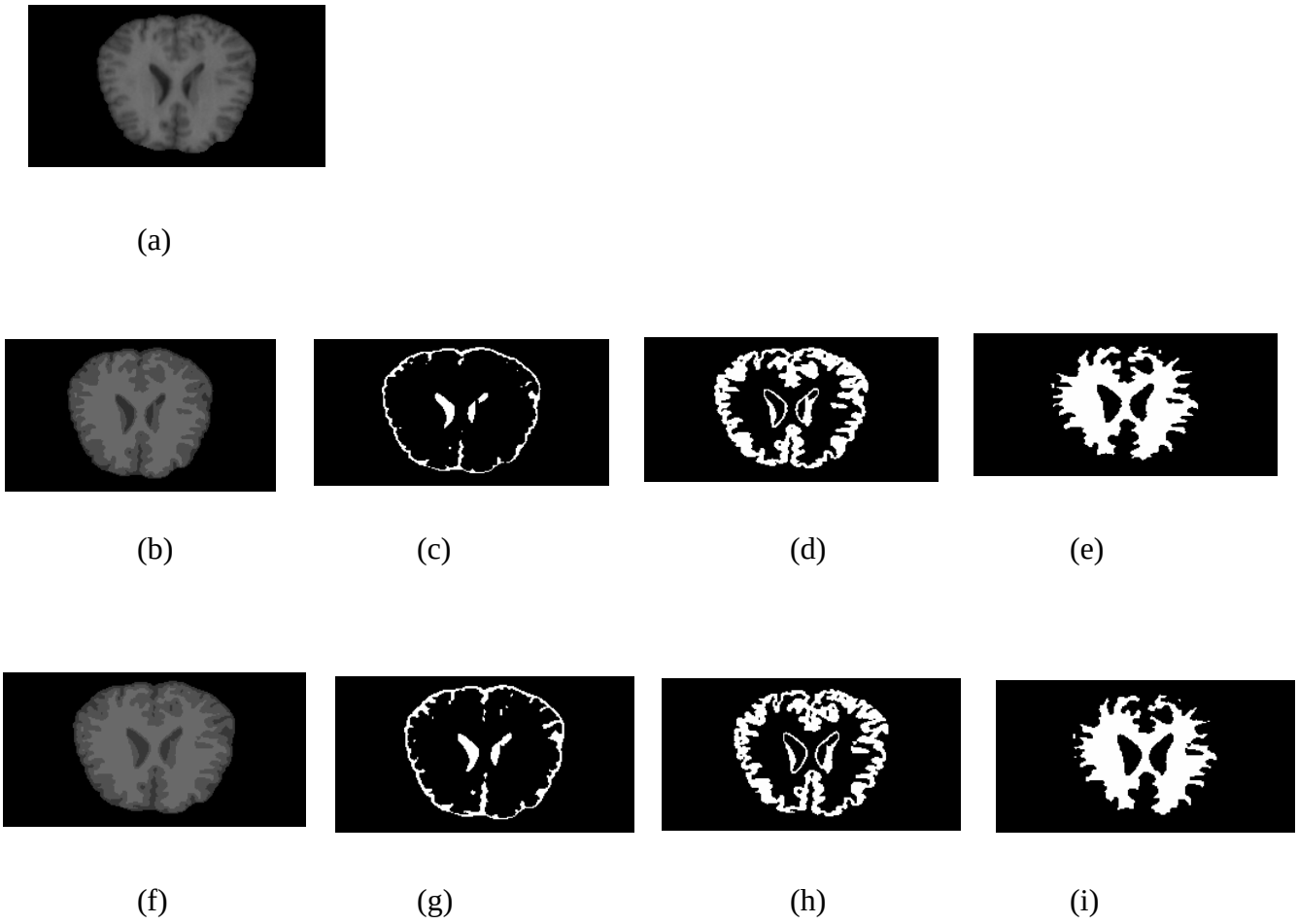

(a)

(b) (c) (d) (e)

(f) (g) (h) (i)

Fig. 19: Qualitative segmented results of the original image, CSF, GM, and WM (from left to right) by the proposed methods on IBSR T1-weighted MR image of volume 05 (a). (b) – (e): method 1 modified; (f) – (i): method 2 modified.

3.2.1.2 Quantitative evaluation

For comparative study quantitative evaluation is essential. We have presented three types of quantitative evaluation based on (i) cluster validity functions, (ii) segmentation accuracy and (iii) tissue segmentation accuracy. The cluster validity functions are presented in terms of (i) partition coefficient, (ii) partition entropy and (iii) similarity index. To reduce the influence of the selected images, results are provided as the average values of 81 images (slice 50 – slice 130) from each volume of the simulated T1 weighted MR brain images.

3.2.1.2.1 Cluster validity functions:

(a) Partition coefficient (V_{pc}):

In Fig. 20 comparative results in terms of V_{pc} for the proposed method 1 modified and method 2 modified over 10 BrainWeb T1-weighted MR brain image volumes with different combination of noise and inhomogeneity are shown. Similarly, in Fig. 21 V_{pc} for the proposed method 1 modified and method 2 modified is compared over three IBSR T1-weighted MR brain image volumes.

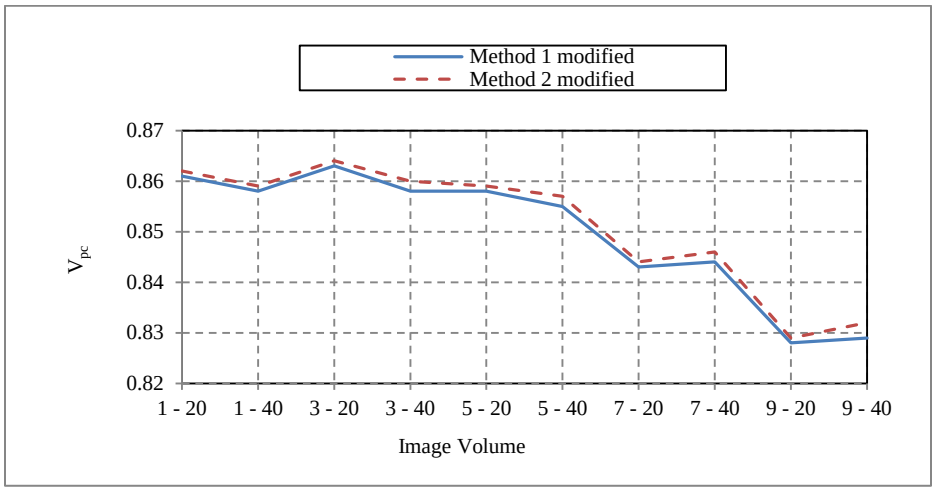

Fig. 20: Comparative study in terms of V_{pc} for the proposed method 1 modified and method 2 modified over 10 BrainWeb T1-weighted MR brain image volumes with different combination of noise and inhomogeneity.

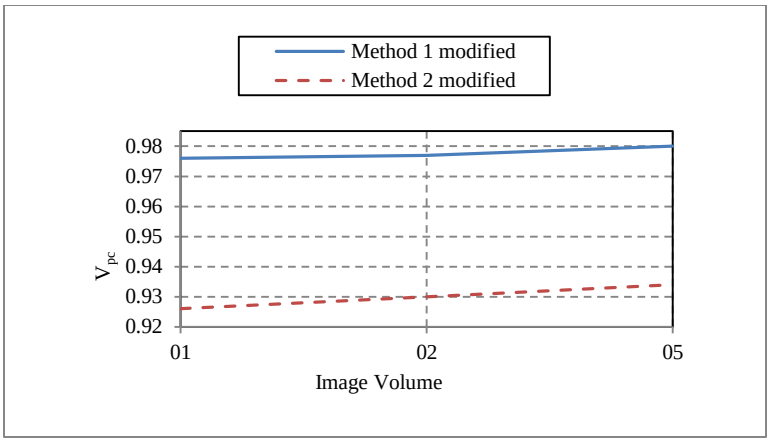

Fig. 21: Comparative study in terms of V_{pc} for the proposed method 1 modified and method 2 modified over 3 IBSR T1-weighted MR brain image volumes.

(b) Partition entropy (V_{pe}):

In Fig. 22 comparative results in terms of V_{pe} for the proposed method 1 modified and method 2 modified over 10 BrainWeb T1-weighted MR brain image volumes with different combination of noise and inhomogeneity are shown. Similarly, in Fig. 23 V_{pe} for the proposed method 1 modified and method 2 modified is compared over three IBSR T1-weighted MR brain image volumes.

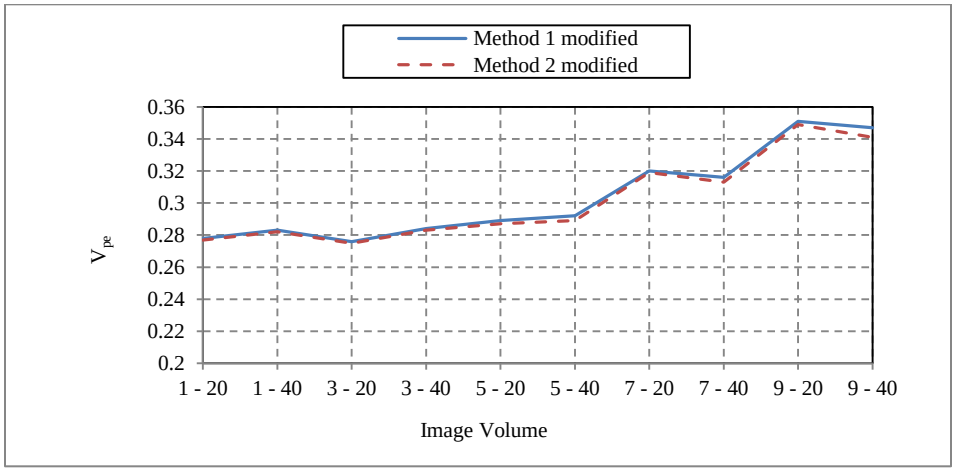

Fig. 22: Comparative study in terms of V_{pe} for the proposed method 1 modified and method 2 modified over 10 BrainWeb T1-weighted MR brain image volumes with different combination of noise and inhomogeneity

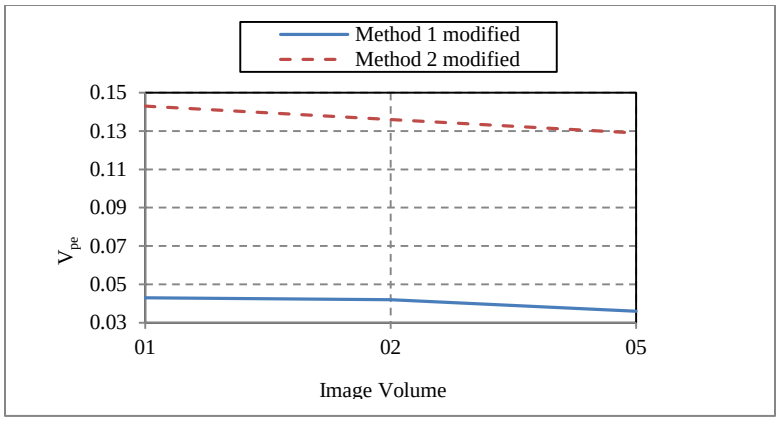

Fig. 23: Comparative study in terms of V_{pe} for the proposed method 1 modified and method 2 modified over 3 IBSR T1-weighted MR brain image volumes.

(c) Similarity index (ρ):

In Fig. 24 comparative results in terms of **ρ** for the proposed method 1 modified and method 2 modified over 10 BrainWeb T1-weighted MR brain image volumes with different combination of noise and inhomogeneity are shown. Similarly, in Fig. 25 **ρ** for the proposed method 1 modified and method 2 modified is compared over three IBSR T1-weighted MR brain image volumes.

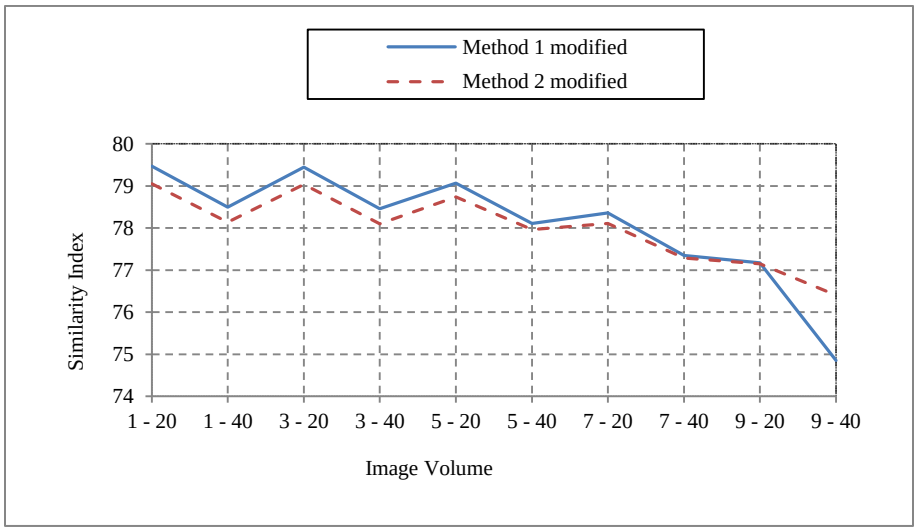

Fig. 24: Comparative study in terms of **ρ** for the proposed method 1 modified and method 2 modified over 10 BrainWeb T1-weighted MR brain image volumes with different combination of noise and inhomogeneity.

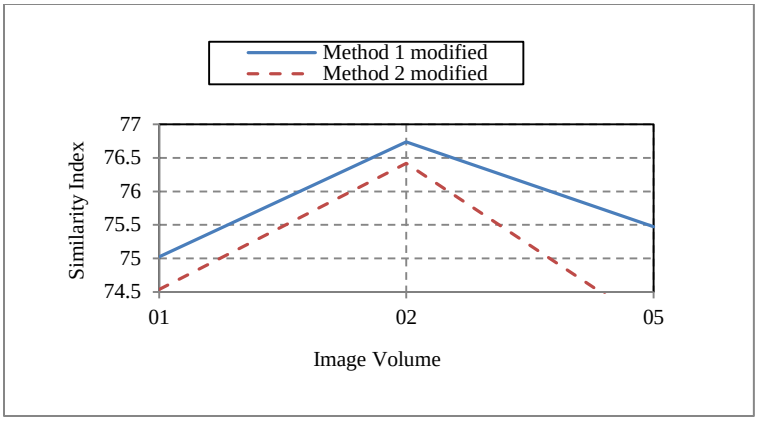

Fig. 25: Comparative study in terms of $\boldsymbol{\rho}$ for the proposed method 1 modified and method 2 modified over 3 IBSR T1-weighted MR brain image volumes.

3.2.1.2.2. Segmentation accuracy (SA):

Table 8 describes the comparative performance of different segmentation algorithms in terms of segmentation accuracy on the 10 BrainWeb T1-weighted MR brain image volumes with different combination of noise and intensity inhomogeneity. Similarly, Table 9 describes the comparative performance of different segmentation algorithms in terms of segmentation accuracy on the 3 IBSR T1-weighted MR brain image volumes.

Table 8:

Comparative performance of different segmentation algorithms in terms of segmentation accuracy on the BrainWeb T1-weighted MR brain image volumes with different combination of noise and intensity inhomogeneity.

Volumes (Noise% - IIH%)	Tissue Regions	Segmentation Accuracy (SA)								
		FCM	FGFCM	sFCM	ASIFC	PFCM	Method 1 modified	Standard deviation	Method 2 modified	Standard deviation
1 – 20	CSF	0.956	0.938	0.966	0.969	0.961	0.924	±0.017	0.914	±0.016
	GM	0.922	0.895	0.938	0.942	0.935	0.943	±0.012	0.928	±0.016
	WM	0.966	0.977	0.975	0.978	0.976	0.971	±0.008	0.981	±0.004
1 – 40	CSF	0.938	0.917	0.944	0.947	0.950	0.924	±0.016	0.913	±0.015
	GM	0.874	0.853	0.931	0.934	0.875	0.930	±0.015	0.913	±0.019
	WM	0.918	0.959	0.968	0.973	0.940	0.938	±0.008	0.955	±0.009
3 – 20	CSF	0.930	0.906	0.938	0.942	0.949	0.926	±0.016	0.915	±0.015
	GM	0.865	0.848	0.927	0.931	0.907	0.939	±0.012	0.923	±0.015
	WM	0.907	0.951	0.956	0.960	0.974	0.965	±0.012	0.979	±0.004
3 – 40	CSF	0.910	0.893	0.921	0.926	0.925	0.925	±0.015	0.913	±0.014
	GM	0.849	0.835	0.922	0.924	0.850	0.926	±0.015	0.908	±0.019
	WM	0.898	0.944	0.947	0.952	0.937	0.932	±0.011	0.953	±0.008
5 – 20	CSF	0.881	0.861	0.907	0.911	0.907	0.920	±0.015	0.909	±0.015
	GM	0.834	0.828	0.916	0.919	0.879	0.930	±0.012	0.915	±0.015
	WM	0.848	0.941	0.938	0.946	0.959	0.954	±0.018	0.973	±0.004
5 – 40	CSF	0.837	0.832	0.861	0.867	0.875	0.919	±0.014	0.908	±0.015
	GM	0.825	0.821	0.909	0.911	0.837	0.919	±0.016	0.904	±0.017
	WM	0.840	0.916	0.926	0.933	0.925	0.919	±0.019	0.948	±0.008
7 – 20	CSF	0.819	0.816	0.852	0.859	0.836	0.903	±0.016	0.894	±0.016
	GM	0.818	0.801	0.902	0.907	0.815	0.915	±0.014	0.900	±0.015
	WM	0.829	0.909	0.912	0.918	0.949	0.942	±0.023	0.966	±0.005
7 – 40	CSF	0.807	0.795	0.849	0.852	0.817	0.902	±0.018	0.892	±0.017
	GM	0.782	0.792	0.895	0.989	0.772	0.907	±0.018	0.890	±0.018
	WM	0.795	0.906	0.903	0.908	0.926	0.901	±0.028	0.940	±0.009
9 – 20	CSF	0.753	0.739	0.827	0.836	0.777	0.876	±0.021	0.868	±0.017
	GM	0.755	0.736	0.871	0.875	0.762	0.899	±0.019	0.884	±0.016
	WM	0.781	0.873	0.897	0.901	0.932	0.917	±0.040	0.955	±0.008
9 - 40	CSF	0.742	0.731	0.824	0.829	0.753	0.874	±0.025	0.868	±0.019
	GM	0.742	0.725	0.862	0.868	0.737	0.887	±0.021	0.875	±0.018
	WM	0.765	0.876	0.873	0.880	0.914	0.827	±0.215	0.929	±0.008

Table 9:
Comparative performance of different segmentation algorithms in terms of segmentation accuracy on the IBSR T1-weighted MR brain image volumes.

Volumes	Tissue Regions	Segmentation Accuracy (SA)								
		FCM	FGFCM	sFCM	ASIFC	PFCM	Method 1 modified	Standard deviation	Method 2 modified	Standard deviation
Vol 1	CSF	0.767	0.752	0.832	0.837	0.726	0.842	±0.023	0.911	±0.044
	GM	0.629	0.613	0.693	0.696	0.620	0.680	±0.051	0.677	±0.054
	WM	0.950	0.948	0.947	0.958	0.955	0.886	±0.017	0.884	±0.025
Vol 2	CSF	0.756	0.745	0.778	0.782	0.737	0.805	±0.122	0.847	±0.103
	GM	0.748	0.729	0.786	0.793	0.732	0.770	±0.064	0.762	±0.063
	WM	0.944	0.951	0.949	0.956	0.954	0.907	±0.013	0.894	±0.014
Vol 5	CSF	0.623	0.611	0.631	0.636	0.611	0.722	±0.076	0.831	±0.063
	GM	0.753	0.749	0.827	0.831	0.799	0.746	±0.057	0.700	±0.049
	WM	0.632	0.758	0.753	0.778	0.775	0.917	±0.018	0.888	±0.016

3.2.1.2.3. Tissue segmentation accuracy (TSA):

Table 10 describes the comparative performance of different segmentation algorithms in terms of tissue segmentation accuracy on the 10 BrainWeb T1-weighted MR brain image volumes with different combination of noise and intensity inhomogeneity. Table 11 describes the comparative performance of different segmentation algorithms in terms of tissue segmentation accuracy on the 3 IBSR T1-weighted MR brain image volumes.

Table 10:

Comparative performance of different segmentation algorithms in terms of tissue segmentation accuracy on the BrainWeb T1-weighted MR brain image volumes with different combination of noise and intensity inhomogeneity.

Volumes (Noise% - IIH%)	Tissue Regions	Tissue Segmentation Accuracy (TSA)								
		FCM	FGFCM	sFCM	ASIFC	PFCM	Method 1 modified	Standard deviation	Method 2 modified	Standard deviation
1 – 20	CSF	0.463	0.465	0.652	0.668	0.452	0.568	±0.046	0.566	±0.050
	GM	0.724	0.720	0.845	0.862	0.720	0.829	±0.016	0.822	±0.017
	WM	0.741	0.738	0.853	0.873	0.741	0.865	±0.055	0.857	±0.064
1 – 40	CSF	0.458	0.462	0.645	0.657	0,427	0.563	±0.046	0.562	±0.051
	GM	0.719	0.715	0.837	0.848	0.691	0.811	±0.017	0.804	±0.018
	WM	0.738	0.731	0.851	0.862	0.729	0.851	±0.051	0.844	±0.061
3 – 20	CSF	0.451	0.458	0.633	0.642	0.451	0.576	±0.046	0.575	±0.050
	GM	0.717	0.711	0.831	0.843	0.710	0.828	±0.017	0.821	±0.017
	WM	0.735	0.731	0.847	0.858	0.730	0.863	±0.055	0.855	±0.065
3 – 40	CSF	0.442	0.447	0.623	0.639	0.424	0.571	±0.047	0.570	±0.051
	GM	0.698	0.691	0.825	0.836	0.684	0.810	±0.017	0.803	±0.018
	WM	0.724	0.719	0.842	0.854	0.720	0.850	±0.051	0.842	±0.062
5 – 20	CSF	0.439	0.442	0.615	0.623	0.494	0.578	±0.047	0.578	±0.050
	GM	0.693	0.689	0.817	0.829	0.690	0.823	±0.016	0.816	±0.016
	WM	0.716	0.714	0.839	0.846	0.717	0.858	±0.057	0.850	±0.065
5 – 40	CSF	0.419	0.426	0.609	0.618	0.414	0.573	±0.049	0.575	±0.051
	GM	0.678	0.673	0.811	0.825	0.672	0.806	±0.016	0.802	±0.017
	WM	0.714	0.712	0.831	0.842	0.711	0.845	±0.054	0.840	±0.061
7 – 20	CSF	0.417	0.421	0.602	0.611	0.418	0.575	±0.049	0.577	±0.050
	GM	0.660	0.654	0.795	0.816	0.651	0.813	±0.016	0.806	±0.016
	WM	0.694	0.691	0.822	0.835	0.690	0.850	±0.059	0.842	±0.066
7 – 40	CSF	0.390	0.392	0.592	0.601	0.397	0.568	±0.050	0.571	±0.051
	GM	0.645	0.637	0.778	0.792	0.629	0.796	±0.017	0.792	±0.017
	WM	0.693	0.689	0.815	0.829	0.684	0.836	±0.056	0.832	±0.063
9 – 20	CSF	0.377	0.381	0.558	0.579	0.366	0.561	±0.052	0.567	±0.050
	GM	0.621	0.613	0.762	0.786	0.605	0.800	±0.017	0.794	±0.017
	WM	0.666	0.664	0.808	0.824	0.660	0.837	±0.064	0.832	±0.067
9 - 40	CSF	0.361	0.372	0.552	0.571	0.358	0.551	±0.055	0.562	±0.051
	GM	0.610	0.605	0.751	0.769	0.590	0.776	±0.025	0.781	±0.017
	WM	0.671	0.670	0.792	0.817	0.662	0.783	±0.206	0.823	±0.064

Table 11:
Comparative performance of different segmentation algorithms in terms of tissue segmentation accuracy on the IBSR T1-weighted MR brain image volumes.

Volumes	Tissue Regions	Tissue Segmentation Accuracy (TSA)								
		FCM	FGFCM	sFCM	ASIFC	PFCM	Method 1 modified	Standard deviation	Method 2 modified	Standard deviation
Vol 1	CSF	0.534	0.537	0.601	0.620	0.633	0.389	±0.074	0.349	±0.094
	GM	0.622	0.619	0.412	0.738	0.608	0.770	±0.036	0.767	±0.039
	WM	0.664	0.657	0.476	0.779	0.650	0.852	±0.029	0.876	±0.045
Vol 2	CSF	0.630	0.633	0.711	0.731	0.629	0.366	±0.086	0.360	±0.083
	GM	0.651	0.642	0.724	0.758	0.640	0.822	±0.035	0.814	±0.034
	WM	0.707	0.689	0.721	0.740	0.701	0.893	±0.043	0.894	±0.041
Vol 5	CSF	0.528	0.538	0.543	0.562	0.569	0.340	±0.051	0.318	±0.054
	GM	0.646	0.632	0.710	0.731	0.733	0.811	±0.037	0.773	±0.030
	WM	0.621	0.618	0.653	0.689	0.681	0.881	±0.054	0.881	±0.051

3.2.2 Real-patient MR images:

3.2.2.1. Qualitative evaluation

Fig. 26 shows the qualitative results of segmentation of T1-weighted real-patient MR brain image (Fig. 26(a)) by the proposed methods. Fig. 26(b)-(e) show the segmented regions of the original image, CSF, GM, and WM, respectively by the proposed method 1 modified; Fig. 26(f)-(i) show the segmented regions of the original image, CSF, GM, and WM, respectively by the proposed method 2 modified.

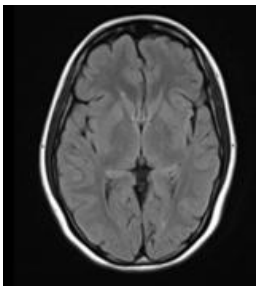

(a)

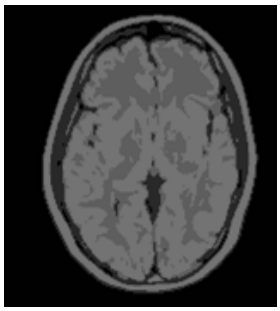

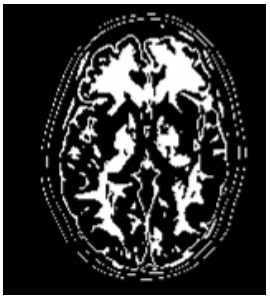

(b) (c) (d) (e)

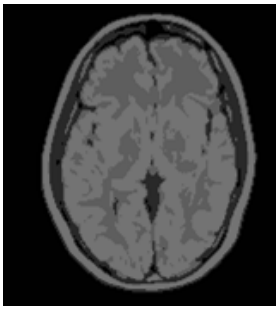

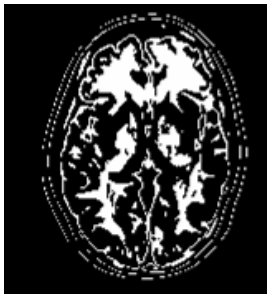

(f) (g) (h) (i)

Fig. 26: : Qualitative segmented results of the original image, CSF, GM, and WM (from left to right) by the proposed methods onT1-weighted real patient MR image (a). (b) – (e): method 1 modified; (f) – (i): method 2 modified.

3.2.2.2. Quantitative evaluation

Table 12 shows the average V_{pc} and V_{pe} values from the three T1-weighted real-patient MR brain image volumes for the method 1 modified and method 2 modified.

Table 12:

Comparative study for different segmentation algorithms of V_{pc} and V_{pe} on three T1-weighted real patient volumes.

Volume	Method	V_{pc}	Standard deviation	V_{pe}	Standard deviation
Real patient 1	FCM	0.791		0.253	
	FGFCM	0.811		0.159	
	sFCM	0.835		0.074	
	ASIFC	0.897		0.056	
	PFCM	0.905		0.053	
	Method 1 modified	0.911	±0.015	0.191	±0.027
	Method 2 modified	0.904	±0.025	0.167	±0.047
Real patient 2	FCM	0.870		0.273	
	FGFCM	0.893		0.193	
	sFCM	0.907		0.178	
	ASIFC	0.922		0.143	
	PFCM	0.935		0.112	
	Method 1 modified	0.913	±0.017	0.186	±0.038
	Method 2 modified	0.921	±0.024	0.167	±0.046
Real patient 3	FCM	0.705		0.558	
	FGFCM	0.815		0.329	
	sFCM	0.886		0.294	
	ASIFC	0.911		0.206	
	PFCM	0.924		0.137	
	Method 1 modified	0.908	±0.012	0.190	±0.023
	Method 2 modified	0.912	±0.012	0.183	±0.024

CHAPTER 4
CONCLUSION

In this project, an “Entropy-based Fuzzy Clustering Algorithm for Brain MR Image Segmentation” has been presented. This method involves Shannon entropy to improve the robustness to the noise and intensity inhomogeneity. This proposed method is examined on ten volumes of simulated T1-weighted brain MR images each one having 81 images and another ten volumes of simulated T2-weighted brain MR images each having 51 images. Finally, for real world application the proposed method is tested on three real patient brain MR image volumes both in qualitative and quantitative manner. The experimental results are compared to the FCM, FGFCM, sFCM, PFCM, ASIFC algorithms. The experimental results show that the method 1 provides superior segmentation results than the method 2 in our proposed methods. Furthermore, the method 1 modified is more tolerant to noise and intensity inhomogeneity than the method 1. The advantage of this proposed method is that it can produce superior segmentation results even in presence of noise and intensity inhomogeneity in MRI data.

CHAPTER 5
REFERENCES

[1] Dilpreet Kaur, Yadwinder Kaur. Various image segmentation techniques: A review. IJCSMC 2014; 3: 809-814.

[2] J.S. Duncan, N. Ayache. Medical image analysis: progress over two decades and the challenges ahead. IEEE Trans. Pattern Anal. Mach. Intell. 2000; 22: 85–106.

[3] Ivana Despotovic, Bart Goossens, Wilfried Philips. MRI segmentation of the human brain: challenges, methods, and applications. Computational and mathematical methods in medicine 2014; 2015.

[4] Sudip Kumar Adhikari, Jamuna Kanta Sing, Dipak Kumar Basu, Mita Nasipuri. Conditional spatial fuzzy C-means clustering algorithm for segmentation of MRI images. Applied Soft Computing 2015; 34: 758-769.

[5] M.A. Balafar, A.R. Ramli, M.I. Saripan, S. Mashohor. Review of brain MRI image segmentation methods. Artif. Intell. Rev. 2010; 33: 261–274.

[6] Dzung L. Pham, Xu Chenyang, Jerry L. Prince. A Survey of Current Methods in Medical Image Segmentation, in: Technical Report JHU/ECE-99-01. Annual Review of Biomedical Engineering 1998.

[7] S.D. Olabarriaga, A.W. Smeulders. Interaction in the segmentation of medical images: a survey. Med. Image Anal. 2001; 5: 127–142.

[8] Li Ma, R.C. Staunton. A modified fuzzy C-means image segmentation algorithm for use with uneven illumination patterns. Pattern Recognit. 2007; 40: 3005–3011.

[9] F.B. Tek, A.G. Dempster, I. Kale. Noise sensitivity of watershed segmentation for different connectivity: experimental study. Electron. Lett. 2004; 40: 1332–1333.

[10] J.C. Bezdek. Pattern Recognition with Fuzzy Objective Function Algorithms. Kluwer Academic Publishers, Norwell, MA, USA, 1981.

[11] W. Pedrycz. Conditional fuzzy C-means. Pattern Recognit. Lett.1996; 17: 625–631.

[12] Y.A. Tolias, S.M. Panas. Image segmentation by a fuzzy clustering algorithm using adaptive spatially constrained membership functions. IEEE Trans. Syst. Man Cybern. A: Syst. Hum. 1998; 28: 359–369.

[13] N.A. Mohamed, M.N. Ahmed, A.A. Farag. Modified fuzzy C-means in medical image segmentation. Proc. IEEE-EMBS 2001; 20: 1377–1380.

[14] M. Ahmed, S. Yamany, N. Mohamed, A. Farag, T. Moriarty. A modified fuzzy Cmeans algorithm for bias field estimation and segmentation of MRI data. IEEE Trans. Med. Imaging 2002; 21: 193–199.

[15] A. Liew, S. Leung, W. Lau. Fuzzy image clustering incorporating spatial continuity. IEE Proc. Vis. Image Signal Process 2000; 147: 185–192.

[16] D.L. Pham, J.L. Prince. An adaptive fuzzy C-means algorithm for image segmentation in the presence of intensity inhomogeneities. Pattern Recognit. Lett. 1999; 20: 57–68.

[17] D.L. Pham. Spatial models for fuzzy clustering, Comput. Vis. Image Underst 2001; 84: 285–297.

[18] A.W. Liew, H. Yan. An adaptive spatial fuzzy clustering algorithm for 3D MR image segmentation. IEEE Trans. Med. Imaging 2003; 22: 1063–1075.

[19] Z. Ji, Q. Sun, D. Xia. A framework with modified fast FCM for brain MR images segmentation. Pattern Recognit. 2011; 44: 999–1013.

[20] X. Wang, J. Bu. A fast and robust image segmentation using FCM with spatial information. Digit. Signal Process 2010; 20: 1173–1182.

[21] S. Krinidis, V. Chatzis. A robust fuzzy local information C-means clustering algorithm. IEEE Trans. Image Process 2010; 19: 1328–1337.

[22] J.C. Noordam, W.H.A.M. Broek. Multivariate image segmentation based on geometrically guided fuzzy C-means clustering. J. Chemom 2002; 16: 1–11.

[23] S. Chen, D. Zhang. Robust image segmentation using FCM with spatial constraints based on new kernel-induced distance measure. IEEE Trans. Syst. Man Cybern. B: Cybern 2004; 34: 1907–1916.

[24] W. Cai, S. Chen, D. Zhang. Fast and robust fuzzy C-means clustering algorithms incorporating local information for image segmentation. Pattern Recognit 2007; 40: 835–838.

[25] Z. Wang, Q. Song, Y.C. Soh, K. Sim. An adaptive spatial information-theoretic fuzzy clustering algorithm for image segmentation. Comput. Vis. Image Underst 2013; 117: 1412–1420.

[26] K.S. Chuang, H.L. Tzeng, S. Chen, J. Wu, T.J. Chen. Fuzzy C-means clustering with spatial information for image segmentation. Comput. Med. Imaging Gr 2006; 30: 9–15.

[27] C. Qiu, J. Xiao, L. Yu, L. Han, M.N. Iqbal. A modified interval type-2 fuzzy C-means algorithm with application in MR image segmentation. Pattern Recognit. Lett 2013; 34: 1329–1338.

[28] A.N. Benaichouche, H. Oulhadj, P. Siarry. Improved spatial fuzzy C-means clustering for image segmentation using PSO initialization, Mahalanobis distance and post-segmentation correction, Digit. Signal Process. 2013; 23: 1390–1400.

[29] S.R. Kannan, R. Devi, S. Ramathilagam, K. Takezaw, Effective FCM noise clustering algorithms in medical images, Comput. Biol. Med. 2013; 43: 73–83.

[30] Liao Liang, Lin Tu-Sheng. A fast spatial constrained fuzzy kernel clustering algorithm for MRI brain image segmentation, in: Proceedings of International Conference on Wavelet Analysis and Pattern Recognition. 2007; 82–87.

[31] D. Selvathi, R. Dhivya. Segmentation of tissues in MR images using modified spatial fuzzy C means algorithm, in: Proceedings of International Conference on Signal Processing, Image Processing and Pattern Recognition. 2013; 1–5.

[32] S.K. Adhikari, J.K. Sing, D.K. Basu, M. Nasipuri, P.K. Saha. Segmentation of MRI brain images by incorporating intensity inhomogeneity and spatial information using probabilistic fuzzy C-means clustering algorithm, in: Proceedings of International Conference on Communications, Devices and Intelligent Systems. 2012; 133–136.

[33] I. Levner and H. Zhang. Classification-Driven Watershed Segmentation. EEE Transactions on Image Processing. 2007; 16: 1437-1445.

[34] Varshika Pandey, Vipin Gupta. MRI Image Segmentation Using Shannon and Non Shannon Entropy Measures. IJAIEM 2014; 3: 41-46.

[35] M.Stella Attkins,Blair T Mackiewich. Fully Automatic Segmentation of the Brain in MRI. IEEE Transactions on Medical Imaging 1998; 17.

[36] Samy Sadek, Sayed Abdel-Khalek. Generalized α-Entropy Based Medical Image Segmentation. Journal of Software Engineering and Applications 2014; 7: 62-67.

[37] Chun Yuan, Shagli Liang. Segmentation of Color Image Based on partial Differential Equation. Fourth International Symposium on Computational Intelligence and Design. 2011.

[38] Brainweb Brain database: http://www.bic.mni.mcgill.ca/brainweb/.

[39] IBSR Brain database: http://www.cma.mgh.harvard.edu/ibsr/.

[40] C.A. Cocosco, V. Kollokian, K.R.K.S. Kwan, A.C. Evans. BrainWeb Online interface to a 3D MRI simulated brain database. Neuroimage 1997; 5: 425-425.

[41] J.C. Bezdek. Cluster validity with fuzzy sets. J. Cybern. 1973; 3: 58–73.

[42] J.C. Bezdek. Mathematical models for systematic and taxonomy, in: Proceedings of Eight International Conference on Numerical Taxonomy San Francisco. 1975; 143–166.